

Award Number: W81XWH-07-2-0121

TITLE: F gxgr o gpv'qh"Vgej pqm { 'hqt"K ci g/I wk gf "Rtqvq"Vj gter {

PRINCIPAL INVESTIGATOR: Zelig Tochner, M00

CONTRACTING ORGANIZATION: University of Pennsylvania,  
Philadelphia PA 19104

REPORT DATE: October'2012

TYPE OF REPORT: Annual

PREPARED FOR: U.S. Army Medical Research and Materiel Command  
Fort Detrick, Maryland 21702-5012

DISTRIBUTION STATEMENT:

Approved for public release; distribution unlimited

The views, opinions and/or findings contained in this report are those of the author(s) and should not be construed as an official Department of the Army position, policy or decision unless so designated by other documentation.

REPORT DOCUMENTATION PAGE			Form Approved OMB No. 0704-0188		
Public reporting burden for this collection of information is estimated to average 1 hour per response, including the time for reviewing instructions, searching existing data sources, gathering and maintaining the data needed, and completing and reviewing this collection of information. Send comments regarding this burden estimate or any other aspect of this collection of information, including suggestions for reducing this burden to Department of Defense, Washington Headquarters Services, Directorate for Information Operations and Reports (0704-0188), 1215 Jefferson Davis Highway, Suite 1204, Arlington, VA 22202-4302. Respondents should be aware that notwithstanding any other provision of law, no person shall be subject to any penalty for failing to comply with a collection of information if it does not display a currently valid OMB control number. <b>PLEASE DO NOT RETURN YOUR FORM TO THE ABOVE ADDRESS.</b>					
1. REPORT DATE (DD-MM-YYYY) 1 October 2012		2. REPORT TYPE Annual		3. DATES COVERED (From - To) 48"Ugr 2011 – 47 Sep 2012	
4. TITLE AND SUBTITLE  Development of Technology for Image-Guided Proton Therapy			5a. CONTRACT NUMBER		
			5b. GRANT NUMBER W81XWH-07-2-0121		
6. AUTHOR(S) Keith Cengel MD PhD, Eric Diffenderfer PhD, Derek Dolney PhD, Simon Hastings, Joel Karp PhD, Alexander Lin MD, Rulon Mayer, Sergei Savin, Jessica Sheehan PhD, Zelig Tochner MD Arnaud Belard, LTC John O'Connell MD  vqej pgtB wr j u0wr gpp0gf w			5d. PROJECT NUMBER		
			5e. TASK NUMBER		
			5f. WORK UNIT NUMBER		
7. PERFORMING ORGANIZATION NAME(S) AND ADDRESS(ES)  University of Pennsylvania Philadelphia PA 19104			8. PERFORMING ORGANIZATION REPORT NUMBER		
9. SPONSORING / MONITORING AGENCY NAME(S) AND ADDRESS(ES)  U.S. Army Medical Research and Materiel Command Fort Detrick, Maryland 21702-5012			10. SPONSOR/MONITOR'S ACRONYM(S)		
			11. SPONSOR/MONITOR'S REPORT NUMBER(S)		
12. DISTRIBUTION / AVAILABILITY STATEMENT  Approved for public release; distribution unlimited					
13. SUPPLEMENTARY NOTES					
14. ABSTRACT This report describes the fifth year of work on the award "Proton Therapy Dose Characterization and Verification" which includes investigation in the following areas: (A) the use of positron emission tomography (PET) to determine the dose deposited by a therapeutic proton beam, (B) studies of the radiobiological effect of proton therapy, and (C) support for matching patients to clinical trials. This report also covers the second year of a continuation award "Development of Technology for Image-Guided Proton Therapy" that focuses on transferring technology currently in conventional radiotherapy systems to the proton treatment rooms, especially that technology related to daily patient localization. A component of both of these awards also supports the work done by the Walter Reed Army Medical Center scientists.					
15. SUBJECT TERMS Radiation Oncology, Proton Therapy, Image-Guided Radiotherapy, PET					
16. SECURITY CLASSIFICATION OF:			17. LIMITATION OF ABSTRACT  UU	18. NUMBER OF PAGES  53	19a. NAME OF RESPONSIBLE PERSON USAMRMC
a. REPORT U	b. ABSTRACT U	c. THIS PAGE U			19b. TELEPHONE NUMBER (include area code)

## Table of Contents

<b>Introduction .....</b>	<b>4</b>
<b>Body .....</b>	<b>5</b>
<b>Appendix I (Quarterly Financial Report) .....</b>	<b>54</b>

## **Introduction**

The overall goal of this multi-year research project in collaboration with the Walter Reed Army Medical Center is to develop the necessary technology to make the Roberts Proton Therapy Center in Philadelphia the most advanced proton radiotherapy center. Award # W81XWH-07-2-0121 comprises phases 4 and 5 of this endeavor and consists of the following projects:

### Phase 4

#### A. Positron Emission Tomography (PET) of proton beams to verify dose deposition

1. PET Detector Development: Design a PET scanner optimized for the application of verifying the dose distribution deposited by proton therapy beams. This includes detector selection, electronic and mechanical engineering, data acquisition, and reconstruction software.
2. Cross-section measurements: Measure positron-emitting isotope production from the primary elements found in tissue and compare to the GEANT4 Monte Carlo simulation program.
3. Determination of elemental composition: The verification of the dose distribution cannot be done directly because the production of isotopes is not easily related to the dose deposited. Instead a Monte Carlo simulation program is used to calculate both dose deposited and isotopes produced and the latter is compared to the measured value. It is critical that the correct elemental composition be used in the simulation for this comparison to work. We are investigating how additional imaging methods, such as dual-energy CT, can help determine the composition.

#### B. Radiobiology and microdosimetry of proton beams

1. Radiobiology studies in the proton beam: Develop techniques to measure the radiobiological effectiveness of the proton beam.
2. Microdosimetry studies in the proton beam: Build proportional chambers to measure the linear energy transfer in a proton therapy field.

### Phase 5

#### A. Apply state-of-the-art localization methods, including cone-beam CT and

#### B. implanted radiofrequency beacons, currently used in conventional radiotherapy to proton radiotherapy.

#### C. Develop a computer program to maximize the efficiency of the proton facility.

## **Body**

The Hospital of the University of Pennsylvania, in collaboration with Walter Reed Army Medical Center, is building the most advanced cancer treatment facility in the world. This is a fully-integrated facility utilizing state-of-the-art imaging and conformal treatment techniques including proton radiotherapy. Research projects with the intent of full implementation of end products are required to reach the full potential of proton therapy. In the original statement of work first of five planned projects were identified, to be implemented on a yearly basis to provide the most advanced cancer treatment facility in the world. Each of these projects will help advance proton therapy worldwide and result in measurable benefits. The projects identified were:

- (1) Multi-leaf collimator (MLC) for use on proton therapy gantries
- (2) Cone Beam CT on the Gantry for localization of target volumes
- (3) Proton Radiography to determine dose and stopping power of various tissues
- (4) Positron Emission Tomography (PET) imaging on the gantry to evaluate dose deposition within tissues irradiated
- (5) Scanning proton beam using adaptive radiotherapy techniques based on implementation of MLC, Cone Beam CT, PET imaging.

A major aim of the entire project is to provide the most advanced radiation therapy to military personnel and their immediate families; the facility opened for patient treatment in January, 2010.

Much of this work has been initiated in earlier phases of this award. Phase 1 concentrated on designing and building a Multi-leaf collimator for use in proton therapy. Phase 2 focused on studying the optimal way to use scanned proton beams. The purpose of Phase 3 was to include the ideas of adaptive radiotherapy techniques and to define the role of imaging in proton therapy including the introduction of on- gantry cone beam CT ( CBCT). The integration of these techniques, redefined as image guided proton therapy (IGPT) and adaptive proton therapy (APT) was a major aim of the phase 3 proposal.

This report concentrates on the fifth year progress on the project titled “Proton Therapy Dose Characterization and Verification” and the fourth year of progress on the award “Development of Technology for Image-Guided Proton Therapy”. The Statement of Work in the approved grant proposals included the following items to be investigated. (Note: to minimize confusion, the years in which we expected to perform the work have been replaced by the fiscal year because there are several separate starting dates.)

#### Phase 4 Scope of Work

Year 1 ending 9/30/2008	<ul style="list-style-type: none"><li>• Develop PET detectors</li><li>• Identify and develop appropriate model systems for preclinical testing proton RBE in the Penn proton beam facility</li><li>• Assemble equipment and develop data analysis software</li><li>• Install and test tablet PCs</li></ul>
Year 2 ending 9/30/2009	<ul style="list-style-type: none"><li>• Design PET scanner</li><li>• Design mechanical gantry</li><li>• Develop data acquisition and electronics</li><li>• Develop image reconstruction algorithm</li><li>• Test and implement cell lines and methods as defined in task 9 with standard photon radiation</li><li>• Build and test tissue-equivalent proportional counters</li></ul>
Year 3 ending 9/30/2010	<ul style="list-style-type: none"><li>• Characterize the performance of the PET instrument</li><li>• Measure positron-emitting isotope production</li><li>• Use dual-energy CT and MRI to determine the composition of materials</li></ul>
Year 4 ending 9/30/2011	<ul style="list-style-type: none"><li>• Measurement of RBE for protons using the Penn proton beam facility</li><li>• Measure LET for scattered and scanned beams</li><li>• Enter forms on tablet PCs</li></ul>

#### Phase 5 Scope of Work

Year 1 ending 9/30/2009	<ul style="list-style-type: none"><li>• Identify a vendor consortium to develop a solution for CBCT on or near the gantry</li><li>• Develop a set of hardware and software specifications for the CBCT system</li><li>• Develop a timeline and detailed cost breakdown for the CBCT project consistent with the clinical needs of the UPHS/WRAMC proton therapy project</li><li>• Evaluate radiation hardness of electronics used in the Calypso localization system</li><li>• Measure radiation field in a proton gantry room that the Calypso will experience</li><li>• Develop deterministic and stochastic models for beam allocation</li><li>• Conduct robustness test for deterministic and stochastic models</li></ul>
-------------------------------	---

Year 2 ending 9/30/2010	<ul style="list-style-type: none"> <li>• Install a prototype Calypso system in the gantry room and test at regular intervals while measuring integral neutron dose</li> <li>• Determine how the Calypso beacons affect the dose distribution using Monte Carlo simulations and measurement</li> <li>• Develop model for patient scheduling</li> <li>• Conduct robustness test for the combined model</li> <li>• Implement production models and deploy models and protocols</li> </ul>
Year 3 ending 9/30/2011	<ul style="list-style-type: none"> <li>• Install CBCT system in gantry room and test using phantoms</li> </ul>

*\* No-cost extension granted for phases 4-5, anticipated completion date October 2013.*

*\* Walter Reed Projects (tissue inhomogeneity, organ motion and quantification, telemedicine) were originally included in phases 1-2, but are now included in phases 4-5.*

## **Progress**

The work over the past year is divided into the following sections:

### **Phase 4**

#### *A. Positron Emission Tomography (PET) of proton beams to verify dose deposition*

The prototype RATX detector system has been moved to the fixed proton beam room for testing, which is currently ongoing.

#### *B. Radiobiology and microdosimetry of proton beams*

1. Continue investigation of the implication of the differential physical LET spectra along a SOBP.
2. Microdosimetry studies in the proton beam: Continued efforts to develop microdosimetry data acquisition, fine tune associated electronics, and validate the proper operation of the TEPC detector.

### **Phase 5**

#### *A. Develop a cone-beam CT that can be used in a proton treatment room*

We have contracted with IBA to develop and install an in-room CBCT system. Our joint work has resulted in the design of a benchtop CBCT system, on which images have been acquired on a phantom to test the acquisition software as well as to evaluate the image quality. The integration of the gantry control system with the new imaging software was successfully tested on the benchtop system. In addition, the benchtop CBCT system was able to achieve phantom CBCT images that were of comparable quality to linac based CBCT systems. We tentatively expect installation of the first gantry CBCT system to occur early in 2013

#### *B. Adapt the Calypso localization system for proton rooms*

A great deal of progress was made in the area of making Calypso more radiation hardened so it could function in the proton treatment rooms.

### *C. Beam allocation and scheduling program*

The conceptual design of this program is complete. The focus will now be on the following tasks: 1) creating a working version of the application that relies on the up-to-date patient schedule and real-time events files to produce real-time beam allocation recommendations, 2) fine-tune the algorithm based on actual scheduling and durations data, 3) investigate the performance of real-time beam allocation heuristics that rely only on the knowledge of what patients are currently in treatment rooms, and 4) create robust patient sequencing recommendations.

## Walter-Reed Projects

### *A. Tissue Inhomogeneity*

Current efforts will support further efforts involving heterogeneous materials. A heterogeneous phantom (air, cork, higher density plastic) has been constructed and will soon be assembled. The heterogeneous phantom will be scanned and x-ray and proton treatment plans will be generated for application. The approaches and code described in the progress report will be applied to the heterogeneous phantom.

### *B. Organ Motion*

There will be continued, ongoing efforts to create the complex dynamic lung phantom for testing and evaluation of the effects of organ motion on delivery of proton therapy.

### *C. Telemedicine*

We recently enrolled the first patient from Walter Reed for treatment with proton therapy via telemedicine. We anticipate that this infrastructure will be used to evaluate, simulate, and treat additional patients over the next year, with plans to use this as a template to enroll patients on disease-site specific clinical trials looking at toxicity and quality-of-life for proton radiotherapy treatments).

Of a planned twelve trials, three have been approved: i) Proton Radiation for Low-Grade Gliomas ii) A Trial of Proton Radiation Therapy Using Standard Fractionation for Low-Risk Adenocarcinoma of the Prostate and iii) A Feasibility Trial of Proton Radiation Therapy or Intensity Modulated Radiation Therapy Using Mild Hypofractionation for Intermediate-Risk Adenocarcinoma of the Prostate

Nine more are planned. We hope that because our trials will essentially be using the same processes, our nine subsequent proton trials (CR ADAs and accompanying DSAs/SSVs) will benefit from a speedier review process.



#### **4.A. PET progress**

In the first quarter, progress was made towards adapting the prototype RATX detector system so that it could be moved to the fixed proton beam room for testing, with completion of design and production of a series of modifications to the existing table. The mounting system and detector bed were designed and modified in order to allow the detector to be used in a clinically active area without risking damage to the system or interfering with clinical activities, and allow navigating in and out of the treatment room.

In the second quarter the prototype was moved to the PCAM facility and re-configured inside the fixed beam room. Detector calibrations were reproduced, demonstrating that the detector was moved safely and without damage. Data was taken using a phantom to confirm the uniformity of reconstruction and to measure the absolute sensitivity of the detector, as a pre-requisite to imaging the proton distribution following radiation., in order to ultimately determine the accuracy with which we can determine the range of the proton dose, and ultimately translate these results from phantoms to humans.

In the third quarter, we corrected calibration problems, resulting in substantially improved quality of image reconstruction. This correction was tested with a 20-cm diameter phantom, which then will enable further studies with large phantoms more representative of patients.

Due to higher than expected clinical downtime at the Roberts Proton Therapy Center during the recent quarter, treatment operating hours for patient care have been routinely extended. As a result, we have had significantly less time than expected to continue work on this project. However, we are optimistic that this issue will be resolved for the next quarter, as clinical operations of the proton center have improved as of late.

We have received quotes and specifications for tissue analog phantom materials to address questions about oxygen isotope production during proton irradiation. Moving forward we will also be measuring a predominantly carbon phantom (polyethylene) and a predominantly oxygen phantom (water gel) to isolate the production of oxygen and carbon isotopes.

#### **4.B. Radiobiology and microdosimetry**

##### **1. Radiobiology**

This year, we have continued to investigate the implications of the differential physical LET spectra along a SOBP and the radiosensitivity of cancer cells. (**Fig 1**).

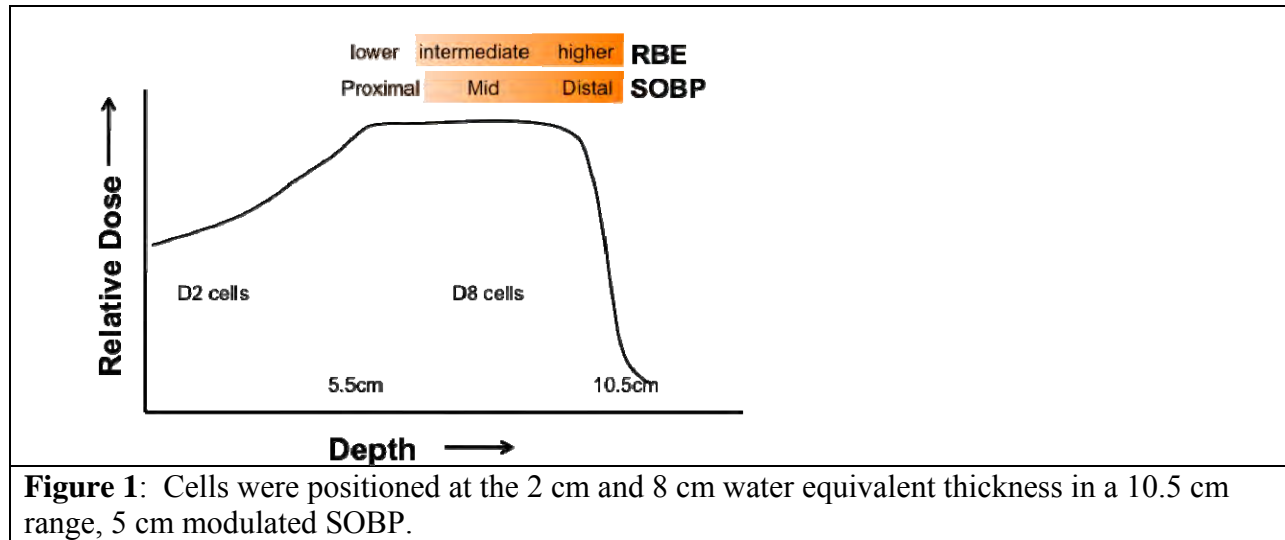


**Figure 1:** Cells were positioned at the 2 cm and 8 cm water equivalent thickness in a 10.5 cm range, 5 cm modulated SOBP.

We have previously found that th at, contrary to our previously stated hypothesis, these highly radioresistant cells do not display a dramatic difference in radiosensitivity for the plateau vs mid-SOBP portions of the proton depth dose distribution (**Fig 2**).

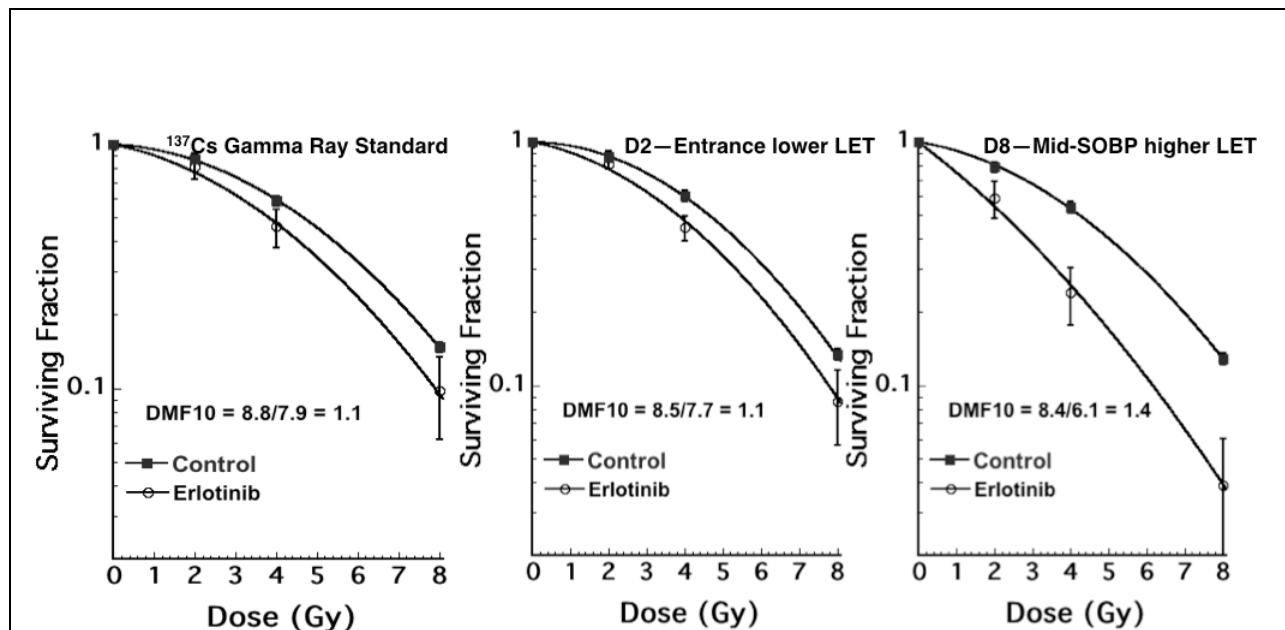


**Figure 2:** Radiosensitivity of SQ20b cells with or without the EGFR inhibitor Erlotinib in high and low LET proton or photons. Clonogenic survival experiments were performed as described in methods and results are presented as mean  $\pm$  sd for experiments performed with a minimum of 6 replicate plates per condition irradiated on the same day.

We will continue to work to extend these observations to determine whether the molecular determinants of radiosensitivity in photon radiation translate to uniform (scalable) changes in radiosensitivity for protons with different LET.

## **2. Microdosimetry**

During the first quarter, the first successful operation of the hand-built miniature tissue equivalent proportional counter (TEPC) in a proton beam was performed. The procedure was repeated for TEPC placements at different solid water depths. Also, the acquired Canberra amplifier and multi-channel analyzer (MCA) system was set up for pulse height analysis operation as a complement for data acquisition and analysis.

The miniature TEPC and Canberra data acquisition system were then used to continue to characterize the neutron dose around the spread out Bragg peak using the dual chamber neutron dosimetry system developed in previous quarters. Continued effort must be expended on developing the microdosimetry data acquisition system, fine tuning the associated electronics, and validating the proper operation of the TEPC detector. However, all of this work is very time consuming with long experiment setup times that are inherent in performing experiments with a complex measurement system. This is coupled with low availability of beam time and altogether it means that the process is time consuming. Even so, we nearly have enough data to produce a first publication describing the TEPC system and relevant measurement data. Measurements with the dual neutron chamber system will proceed relatively quickly and we can anticipate producing one or two more publications that present measurements of secondary neutron dose using the 3 different treatment modalities (passive scattering, uniform scanning, and pencil beam scanning) available at the proton center.

## **Phase 5**

### **A. CBCT project**

#### **A. Development of Cone-Beam CT**

During the last quarter, the performance of the CBCT design was evaluated on a benchtop system with the new X-ray source and detector panel. Using an identical geometrical setup as the proton gantry, CBCT was acquired on a phantom to test the acquisition software as well as to evaluate the image quality. This benchtop system allowed IBA to evaluate the X-ray source and imaging panel, tweak the image reconstruction software and optimize the image quality. The integration of the gantry control system with the new imaging software was successfully tested on the benchtop system. In addition, the benchtop CBCT system was able to achieve phantom CBCT images that were of comparable quality to linac based CBCT systems. Penn is working closely with IBA to use these benchtop CBCT images as benchmarks to define image quality metrics in the acceptance procedure of the first gantry CBCT system upon installation. We tentatively expect installation of the first gantry CBCT system to occur early in 2013.

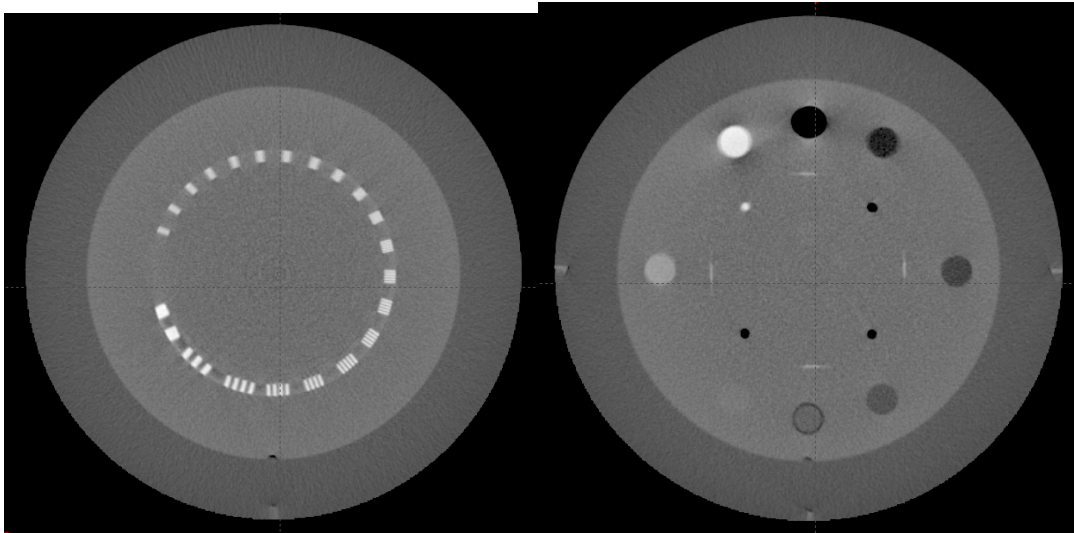
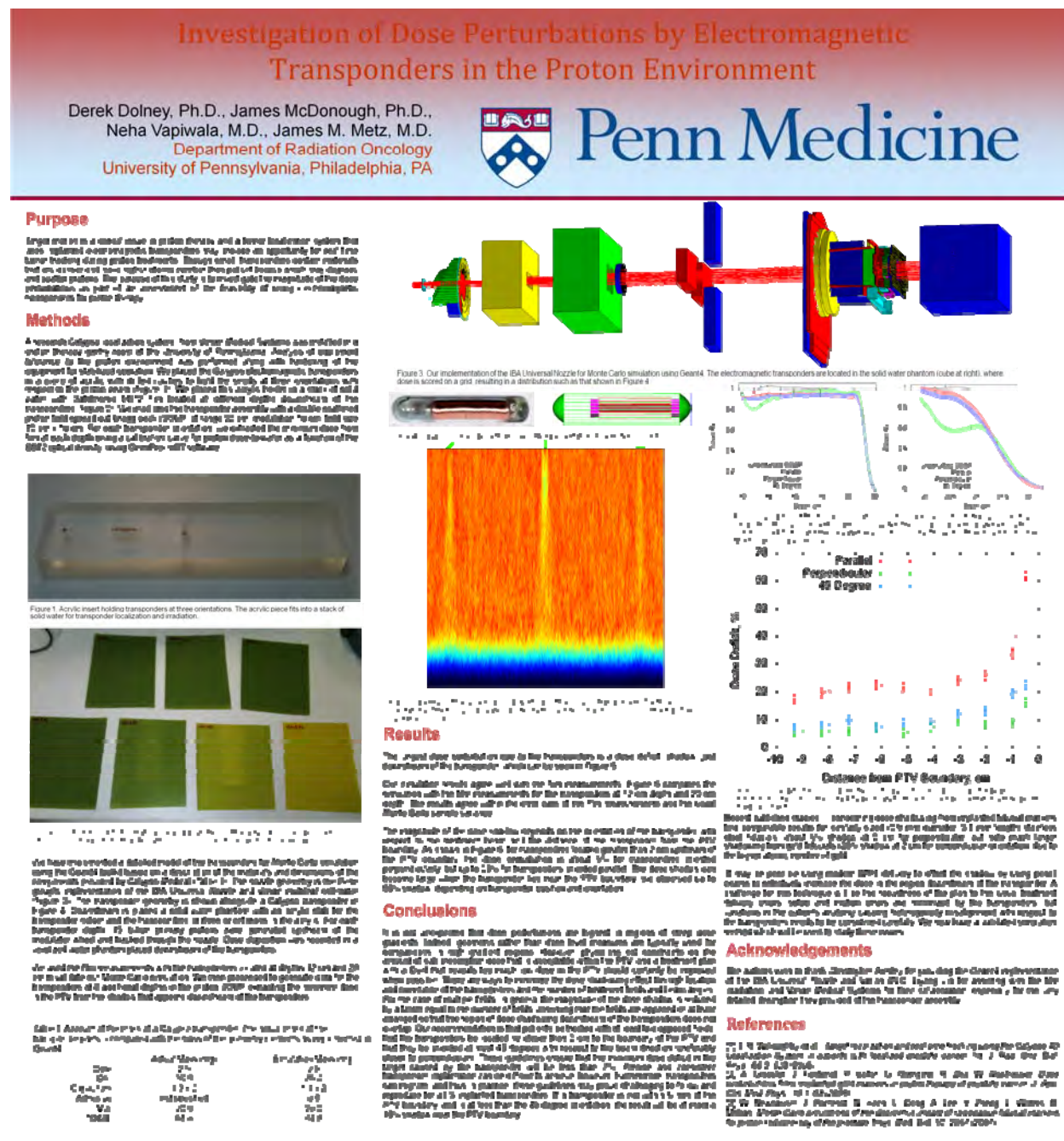


Figure 1. Benchtop CBCT images of a phantom used to evaluate the resolution (left) and Hounsfield number accuracy (right). These images are used to evaluate the image reconstruction software and serve as benchmarks for our gantry CBCT system.

Over the next 2 quarters, we will continue to work closely with IBA with benchtop CBCT images as benchmarks to define image quality metrics in the acceptance procedure of the first gantry CBCT system upon installation. There will be additional calibration tests performed prior to deployment for clinical use. We tentatively expect installation of the first gantry CBCT system to occur early in 2013.

### **B. Implanted RF beacons (Calypso)**

During the past year, we have completed the simulation portion of the project. The results of the study investigating the effect of Calypso radio diotransponders on the dose distribution were presented in poster form at the American Radium Society Meeting. The poster is shown below.



The manuscript with these results has been submitted to Physics in Medicine and Biology.

## C. Beam allocation and patient scheduling project



## **Progress Report for the Proton Beam Allocation Project**

**October 23, 2012**

This report covers our activity during the period of May-October 2012. We have made progress on three fronts: designing the real-time beam allocation application, building a simulation study focused on investigating the performance of beam allocation algorithms under stochastic durations of preparation and field times, and studying the influence of different patient sequencing schemes on throughput performance.

### **1. Designing the real-time beam allocation application.**

Three sources of information are used for making real-time beam allocation decisions: 1) files containing the duration of preparation and field phases for each treatment protocol, 2) the file containing up-to-date patient scheduling information, and 3) the file containing the records of real-time events in each treatment room. Below we provide a description of each of these information sources and discuss how the beam allocation application can operate in real time.

#### **1.1. Protocol durations files.**

One of the issues that need to be addressed in designing the beam allocation application is how to model random durations of preparation and field phases for each treatment protocol. In particular, it is necessary to store data on those durations in a manner that can account for their random nature. An approach for storing these data that we adopt consists of defining, for each preparation or field duration for each treatment protocol, a number of “time buckets” covering time intervals from smallest to largest possible duration.

For example, consider an initial preparation phase for a treatment of “Prostate-2” patients (treatment protocol with 2 fields and prostate as an application site). Suppose that the minimum possible duration for this preparation phase is 1 minute and the maximum possible duration is 30 minutes. In order to store the data for actual durations of this preparation phase, we can define time buckets of size, for example, 0.1 minute, such that the entire interval between 1 minute and 30 minutes is covered by these buckets. In particular, in this case there will be 290 time buckets, with 1<sup>st</sup> one covering the time interval [1, 1.1) minutes, the 2<sup>nd</sup> one – interval [1.1, 1.2), etc., and the last one covering the time interval [29.9, 30) minutes. Each time the actual duration falls within a particular bucket, the “count” of durations in this bucket is increased by 1. Thus, all realization of the actual duration of this preparation phase observed by a given moment in time can be expressed similar to the example in the following Table.

Time Bucket (in mins), $i$	Duration Count, $c_i$
[1, 1.1)	1
[1.1, 1.2)	5
...	...
[29.9, 30)	1

**Table 1. An example of duration counts in each time bucket.**

Such an approach to storing realizations of random durations is equivalent to recording an “empirical” probability distribution of a particular duration. For example, if we use  $N$  buckets to record a particular duration, and the current duration counts for each bucket are  $(c_1, \dots, c_N)$ , we can define the probability that the random duration “falls” within bucket  $i$  as

$$p_i = \frac{c_i}{c_1 + \dots + c_N}, i = 1, \dots, N.$$

If the bucket size is small (e.g., 0.1 mins), we can approximate a given duration as being a random variable taking values equal to the midpoints  $m_i$  of each bucket<sup>1</sup>  $i$  with probabilities given by the above formula. Such probability model can be used to calculate various parameters used during real-time beam allocation. For example, the expected value of such duration can be estimated as

$$E = \sum_{i=1}^N p_i m_i = \frac{c_1 m_1 + \dots + c_N m_N}{c_1 + \dots + c_N}.$$

Duration observations for any field or preparation phase for any protocol can be stored in this way and then used during real-time beam allocation.

Protocol data files are created with the help of users who set the appropriate time-bucket size, and the maximum and minimum preparation and field duration parameters. As new treatment protocols are created, the corresponding protocol data files are added to the overall set of files. Realistic estimates for the initial duration counts should also be specified at the time a particular protocol data file is created.

All protocol data files are read at the beginning of each day, with the appropriate duration metrics (such as expected durations) calculated and stored for use during real-time beam allocation. Protocol data files are updated at the end of each day by adding duration counts for all observed preparation phases and fields to the appropriate files.

## 1.2. Patient Schedule file.

A Daily Schedule file (we assume it is presented in a CSV format) contains up-to-date information on the actual patients served up to the current moment and anticipated patients to be served from the current moment till the end of the day in each treatment room. The information includes scheduled patient arrival times and treatment protocols. The “up-to-date” feature implies that the initial schedule available in the beginning of the day and is automatically updated during the day in cases of patient no-shows, cancellations and new additions to the schedule. For each treatment room, a Daily Schedule file contains a list of patient scheduled arrival times and treatment protocols. An example of a Daily Schedule file is given in Table 2 below. In this example, the 1<sup>st</sup> patient to arrive at room 1 is scheduled for 8:00am and is to be served according to the treatment protocol 1, the next one is scheduled for 8:30am and is to be served according to the treatment protocol 7, etc.

---

<sup>1</sup> For example, the midpoint of the time bucket  $[1, 1.1)$  is  $m_1 = 1.05$ , and the midpoint of the time bucket  $[29.9, 30)$  is  $m_{290} = 29.95$ .



Room	Arrival	Protocol	Arrival	Protocol	Arrival	Protocol	Arrival	Protocol	Arrival	Protocol	Arrival	Protocol
1	480	1	510	7	540	1	570	4	600	2	630	2
2	480	2	510	5	540	1	570	3	600	1	630	3
3	480	2	510	3	540	3	570	13	600	12	630	1
4	480	3	510	4	540	2	570	10	600	1	630	5
5	480	1	510	1	540	1	570	1	600	1	630	9

**Table 2. Example of a Patient Schedule file.**

### 1.3. Real-Time Events file.

The Real-Time Events file stores (we assume, in the CSV format) information on patient-related and beam-related events since the beginning of the day up to the present moment. For each event, three pieces of information are recorded: “time stamp”, “treatment room”, and “event type”. The “time stamp” records the time at which a particular event happened (expressed, for example, in minutes since midnight). The “treatment room” is the number of room in which event happened. The “event type” describes one of (currently 5) possible events of importance to the beam allocation algorithm:

Event type 1 = “Patient has entered the treatment room”

Event type 2 = “Patient is ready for the beam”

Event type 3 = “Beam has been delivered to the room”

Event type 4 = “Beam has been returned from the room”

Event type 5 = “Patient has left the room”

An example of the Real-Time Events file is shown in Table 3 below.

Time Stamp	Room	Event Type
480	1	1
480	2	1
480	3	1
480	4	1
480	5	1
483.1	2	2
483.5	1	2
483.6	2	3
484.5	2	4
484.7	1	3
485.2	4	2
486.3	1	4
487.5	5	2

**Table 3. An example of a Real-Time Events file.**

In this example, the sequence of events is as follows: at 8:00am 5 patients enter rooms 1 through 5. Next, at 8:03:06am the patient in room 2 is ready for the beam, followed by a patient in room 1 that becomes ready for the beam at 8:03:30am. The beam is delivered to room 2 at 8:03:36am



and is returned at 8:04:30am. Beam is then delivered to room 1 at 8:04:42am. Next, the patient in room 4 gets ready for the beam at 8:05:12am. The beam is returned from room 1 at 8:06:18am. Finally, patient in room 5 gets ready for the beam at 8:07:30am.

#### **1.4. How the beam-allocation application operates in real time.**

It is assumed that when the beam allocation algorithm is invoked in real time, there is at least one room waiting for the beam. If there is only a single room waiting for the beam, the beam will be sent to that room. If there are two or more rooms waiting for the beam, the beam allocation algorithm will read the contents of the Daily Schedule and Real-Time Events files and will convert the information in these two files into the current “state” of the treatment system, representing a sequence of preparation and field times remaining to be delivered in each treatment room at a time when a beam allocation decision needs to be made, as well as the waiting time, if any, incurred so far by the next field ready to be served in each room. The idea behind a real-time single-field dynamic beam allocation algorithm (RTSFD) is based on analyzing the throughputs resulting from sending the beam to each of the currently waiting rooms, followed by first-ready first-serve beam allocation (FRFS) afterwards. In other words, the RTSFD algorithm operates on the assumption that all preparation and field durations are known with certainty. In the deterministic setting, comparison between the alternative beam trajectories takes very little time for any realistic number of fields/patients remaining to be served at the time the allocation is made. On the other hand, if the values of future preparation and field durations are random (and known only in distribution, as described in protocol data files), the goal of minimizing the throughput has to be adjusted, for example, to a goal of minimizing the expected throughput. In such settings, the task of calculating the expected throughput resulting from following a FRFS beam allocation approach is actually hard to accomplish, especially in real time, since the FRFS beam trajectory itself depends on the actual values of preparation and field durations. One adaptation of the deterministic version of the RTSFD algorithm to stochastic settings is, when making a beam allocation decision, to approximate the future (random) preparation and field durations by their expected values. Note that when a beam allocation decision is made in real time, the decision maker knows the actual values of the waiting times for those patients that are ready for the beam, and the elapsed preparation durations for those patients that have not yet completed their preparation phases. The idea of a “mixed” state of the system stems from the amount of information available to the decision maker at the time the beam allocation has to be made: the exact values of waiting and elapsed preparation durations as well as the distributional information on the remaining future preparation and field durations.

Once the mixed state of the treatment system is calculated, it is passed on to the beam allocation algorithm (such as RTSFD algorithm) that calculates which room should receive the beam next. Given that the Real-Time Events file records all beam and patient-service related events, at the end of each day it is possible to provide an analysis of the effect of alternative beam allocation approaches, such as FRFS.

## 2. Simulating the performance of beam-allocation algorithms under different patient sequences and stochastic durations.

At present, we have built a portfolio of alternative real-time beam allocation algorithms and in the past several months we have designed a simulation to test the performance of these algorithms under different patient sequences and deterministic and stochastic durations of the preparation and field phases for each treatment protocol. Below we report the results of several such test studies.

### 2.1. Data used in the numerical tests.

In our numerical tests we have used the data from the “Dataset 2” collected during the summer of 2010. This dataset represents the field and preparation durations for the treatment protocols shown in Table 4. The “% of Patients” field represents the fraction of patients treated according to a particular protocol.

Protocol	Site	Fields	% Patients
1	Prostate	2	49.73
2	Brain	2	5.41
3	Brain	3	20.54
4	Chest	2	3.78
5	Lung	2	3.24
6	Forearm	2	2.7
7	Sacrum	2	3.24
8	Spine	2	3.24
9	Sternum	2	2.16
10	Abdomen	2	1.62
11	Pelvis	2	1.08
12	Thymoma	2	1.63
13	Sacrum	3	1.63

**Table 4. Treatment protocols used in the numerical study.**

Using these treatment protocols, we have generated random daily patient sequences using the probabilities based on the % fractions from Table 4. For each daily patient sequence, we have assumed that the first patient arrives to each treatment room at 9:00am, and that each following patient enters a treatment room immediately after the departure of the previous patient. Table 5 shows an example of a randomly generated patient sequence with 15 patients in each treatment room.

Room	Patient 1	Patient 2	Patient 3	Patient 4	Patient 5	Patient 6	Patient 7	Patient 8	Patient 9	Patient 10	Patient 11	Patient 12	Patient 13	Patient 14	Patient 15
1	1	1	1	1	4	2	3	3	1	1	1	1	2	7	1
2	1	3	3	1	3	4	1	1	3	1	1	12	7	4	3
3	1	1	2	1	1	11	3	13	7	3	1	1	3	1	1
4	1	1	1	1	3	1	3	1	1	1	1	3	3	12	1
5	1	3	1	1	12	1	1	1	3	1	11	6	3	2	2

**Table 5. An example of a daily patient sequence with 15 patients in each room.**

In our numerical tests we have used both the deterministic and the stochastic durations of each preparation and field phase for each of the protocols in Table 4. In the “deterministic” experiments we have used the durations shown in Table 6.

Protocol	Name	Prep Phase 1	Field 1	Prep Phase 2	Field 2	Prep Phase 3	Field 3	Prep Phase 4
1	Prostate-2	7.8	1.4	3.7	1.4	2.8	N/A	N/A
2	Brain-2	11.7	0.7	3.3	1.0	3.4	N/A	N/A
3	Brain-3	10.9	0.6	3.4	0.4	3.5	0.4	3.2
4	Chest-2	13.2	1.2	2.9	0.6	2.2	N/A	N/A
5	Lung-2	12.4	0.6	3.0	0.7	3.5	N/A	N/A
6	Forearm-2	12.1	0.8	4.4	0.9	3.4	N/A	N/A
7	Sacrum-2	11.8	0.7	2.6	0.8	2.5	N/A	N/A
8	Spine-2	11.0	1.1	5.0	1.4	4.6	N/A	N/A
9	Sternum-2	10.0	1.0	4.1	0.7	2.2	N/A	N/A
10	Abdomen-2	18.3	0.5	3.7	0.5	3.9	N/A	N/A
11	Pelvis-2	11.5	0.5	3.6	0.5	2.1	N/A	N/A
12	Thymoma-2	6.0	0.3	3.8	1.3	2.6	N/A	N/A
13	Sacrum-3	12.4	0.5	2.7	0.4	1.1	0.4	3.5

**Table 6. Expected durations (in minutes) of preparations and field phases for 13 treatment protocols.**

In the “stochastic” experiments we have used the actual recorded durations, with expectations corresponding to the ones in Table 6. Below we report the results of both deterministic and stochastic numerical tests.

## 2.2.Deterministic durations.

In our numerical tests, in addition to testing the performance of the RTSFD algorithm, we have also focused on investigating the effectiveness of a simpler version of this beam allocation algorithm, namely, the one that applies the RTSFD approach only to the patients that are currently in the treatment rooms. We call this algorithm Real-Time Patients-In-Room, or RTPIR. The advantage of using RTPIR is in the fact that it utilizes a much shorter planning horizon, and, thus, relies on a much smaller information set.

### 2.2.1. RTSFD vs. RTPIR: fixed patient sequences.

As an initial check, we have applied both the RTSFD and RTPIR to 1000 randomly generated patient sequences consisting of  $N=1$  patient in each room. By construction, both algorithms are producing identical results in this case. In our tests, we have kept track of 3 performance measures for each algorithm: throughput (time required to complete the last field of the last patient), the total patient waiting time (sum of all times spent by all patients waiting for the beam), and the maximum patient waiting time (the largest amount of time spent by any patient waiting for the beam). Note that since the total sum of all fields for all patients does not depend on the chosen beam allocation rule, the throughput minimization is



equivalent to minimizing the beam idle time, i.e., the total amount of time beam spends waiting for some patient to get ready. The results of these tests are presented in Table 7.

	Throughput RTSFD	Throughput RTPIR	Total Patient Wait RTSFD	Total Patient Wait RTPIR	Max Patient Wait RTSFD	Max Patient Wait RTPIR
Average Gap	0.029	0.029	0.009	0.009	-0.052	-0.052
St.Dev. Gap	0.041	0.041	0.025	0.025	0.104	0.104
Max Gap	0.129	0.129	0.227	0.227	0.264	0.264
Min Gap	0.000	0.000	-0.179	-0.179	-1.040	-1.040

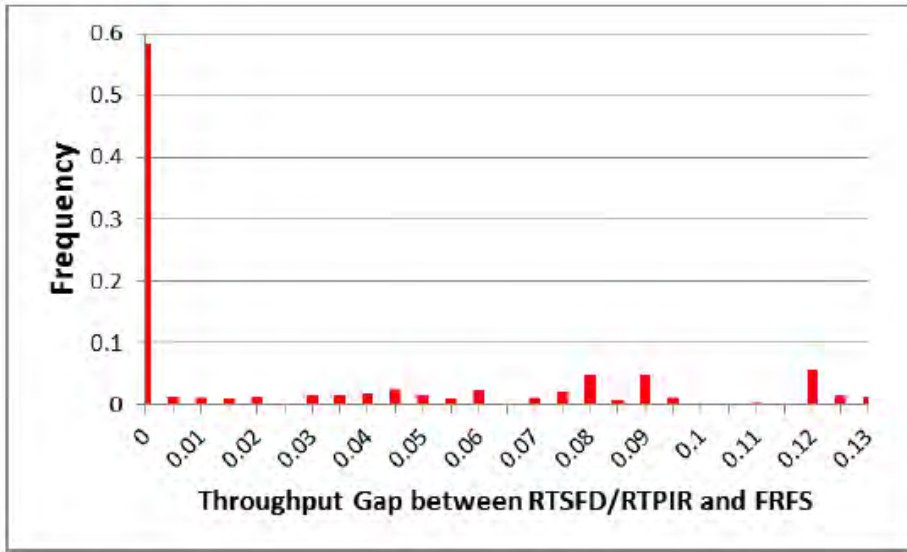
  

	Gap T RTSFD	Gap T RTPIR	Gap W RTSFD	Gap W RTPIR	Gap Max W RTSFD	GAP Max W RTPIR
Gap T RTSFD	1.00					
Gap T RTPIR	1.00	1.00				
Gap W RTSFD	0.53	0.53	1.00			
Gap W RTPIR	0.53	0.53	1.00	1.00		
Gap Max W RTSFD	-0.64	-0.64	-0.33	-0.33	1.00	
GAP Max W RTPIR	-0.64	-0.64	-0.33	-0.33	1.00	1.00

**Table 7. Performance of RTSFD and RTPIR for  $N=1$  patient in each treatment room (1000 randomly generated patient schedules, deterministic durations).**

As expected, both algorithms result in the same performance – on average (for a randomly selected patient schedule), they result in 2.9% improvement in generated throughput as compared to FRFS. In addition, both algorithms generated small (0.9%) reduction in total patient wait time, while increasing the maximum patient wait time, on average, by 5.2%. It is not surprising that the maximum patient wait time increases when beam allocation deviates from FRFS approach that allocates the beam to patient with the longest wait. A similar message is contained in the correlation matrix: throughput reduction is positively correlated with the reduction in total patient waiting time and negatively correlated with the reduction in maximum patient waiting time.

However, it is important to note that the actual patient sequences, of course, are not random and can be selected to maximize the impact of real-time beam allocation. As Table 7 indicates, the throughput improvement can vary from non-existent to 12.9%. Figure 8 shows the distribution of the throughput improvement for RTSFD and RTPIR in this case.



**Figure 8. Distribution of the throughput performance gap for RTSFD and RTPIR algorithms (1000 randomly generated patient schedules with  $N=1$  patient in each treatment room, deterministic durations).**

Next, we conducted tests for patient sequences that include  $N=2$  patients in each room. Table 9 reports the results on these tests.

	Throughput RTSFD	Throughput RTPIR	Total Patient Wait RTSFD	Total Patient Wait RTPIR	Max Patient Wait RTSFD	Max Patient Wait RTPIR
Average Gap	0.030	0.014	0.089	-0.008	-0.321	-0.063
Std.Dev. Gap	0.024	0.023	0.090	0.076	0.331	0.131
Max Gap	0.120	0.093	0.341	0.340	0.356	0.318
Min Gap	0.000	-0.067	-0.196	-0.348	-1.844	-1.072

	Gap T RTSFD	Gap T RTPIR	Gap W RTSFD	Gap W RTPIR	Gap Max W RTSFD	GAP Max W RTPIR
Gap T RTSFD	1					
Gap T RTPIR	0.60347058	1				
Gap W RTSFD	0.42069701	0.091724481	1			
Gap W RTPIR	0.19121344	0.272998989	0.369948631	1		
Gap Max W RTSFD	-0.34371277	-0.039513219	-0.384679765	0.045792966	1	
GAP Max W RTPIR	-0.02326322	-0.139525213	0.110826305	0.21533004	0.15278711	1

**Table 9. Performance of RTSFD and RTPIR for  $N=2$  patient in each treatment room (1000 randomly generated patient schedules, deterministic durations).**

As we observe, that performance of the RTSFD algorithm remains largely unchanged, with the average throughput performance improvement of 3.0%, and the maximum improvement of 12%. However, the performance of the RTPIR algorithm decreases to an average 1.4% improvement in throughput (with maximum improvement of 9.3%). Note that the worst-case performance of the RTPIR is an increase of 6.7% in the throughput as compared to FRFS. The correlation between the throughput gaps generated by RTSFD and RTPIR algorithms is 60%. Figure 10 shows the distribution of the throughput performance gap for the RTSFD

algorithm. As we observe, the proportion of cases in which RTSFD manages to generate an improvement over FRFS increases from 41.7% to 91.4%.

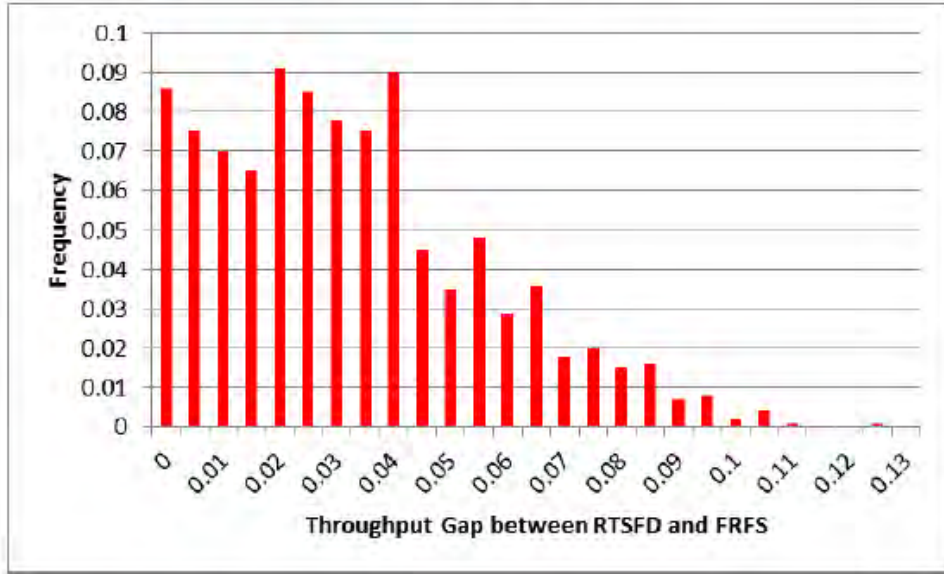


**Figure 10. Distribution of the throughput performance gap for RTSFD and RTPIR algorithms (1000 randomly generated patient schedules with  $N=1$  patient in each treatment room, deterministic durations).**

As the next step, we have created patient sequences with up to  $N=15$  patients in each treatment room. Figure 11 shows how the average (over 1000 random patient sequences generated for  $N=1, 2$ , and over 100 random patient sequences generated for  $N=3, \dots, 15$ ) throughput gap (as compared to FRFS) changes with  $N$  for RTSFD and RTPIR algorithms.

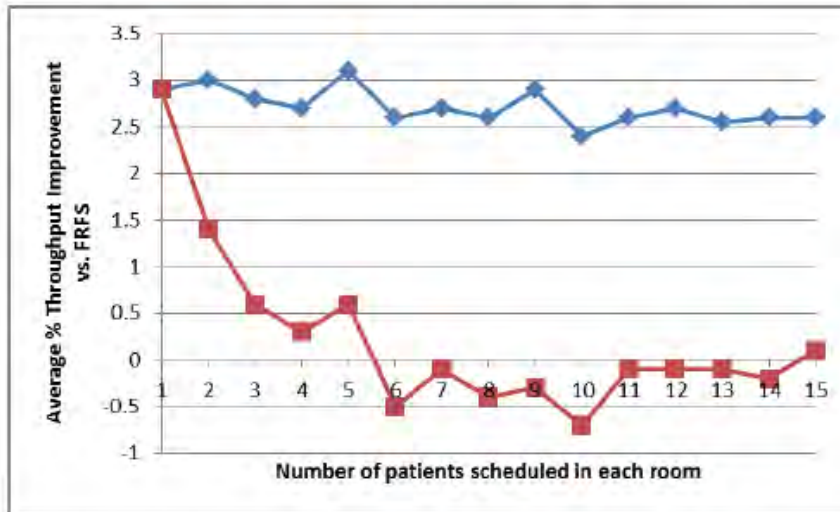




**Figure 11. Average throughput gap for RTSFD and RTPIR vs. FRFS algorithms as a function of number of patients scheduled in each treatment room,  $N$  (deterministic durations).**

As Figure 11 indicates, the average RTSFD performance is not substantially affected by the number of scheduled patients and remains between 2.5% and 3%. At the same time, average RTPIR performance drops as the number of scheduled patients increases. In particular, as  $N$  reaches 6, the average performance of the RTPIR drops to 0%. It is important, however, to also keep in mind that the choice of the patient sequence can significantly affect the performance of a particular algorithm. Figure 12 shows how the maximum throughput improvement values depend on the number of patients scheduled in each treatment room.

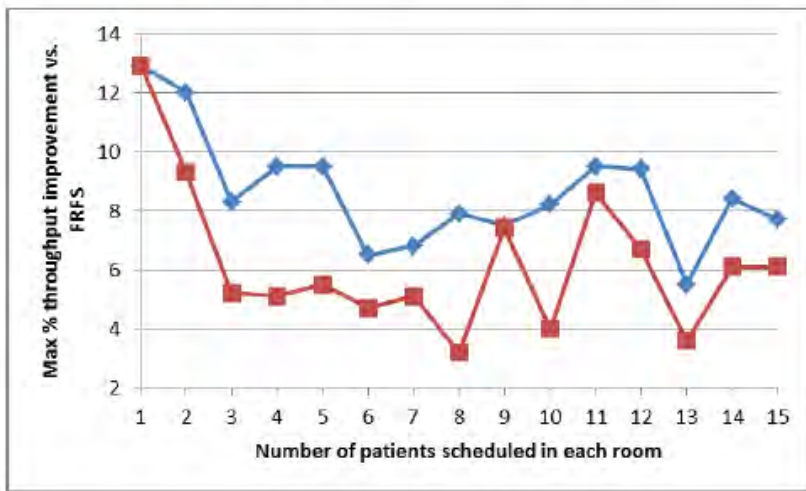


**Figure 12. Maximum throughput gap for RTSFD and RTPIR vs. FRFS algorithms as a function of number of patients scheduled in each treatment room,  $N$  (deterministic durations).**

As we observe from Figure 12, for  $N > 1$  patients per room, best RTSFD performance (over throughput generated by FRFS) is in the 5%-12% range, while best RTPIR performance is in the 3%-9% range.

It is interesting to look at how such throughput improvements can be translated into increases in the number of patients served each day. Figure 13 shows how the average (over 100 random patient sequences) throughput generated by a FRFS policy changes when the number of patients scheduled in each room increases from  $N=1$  (5 total scheduled patients) to  $N=15$  (75 total scheduled patients).

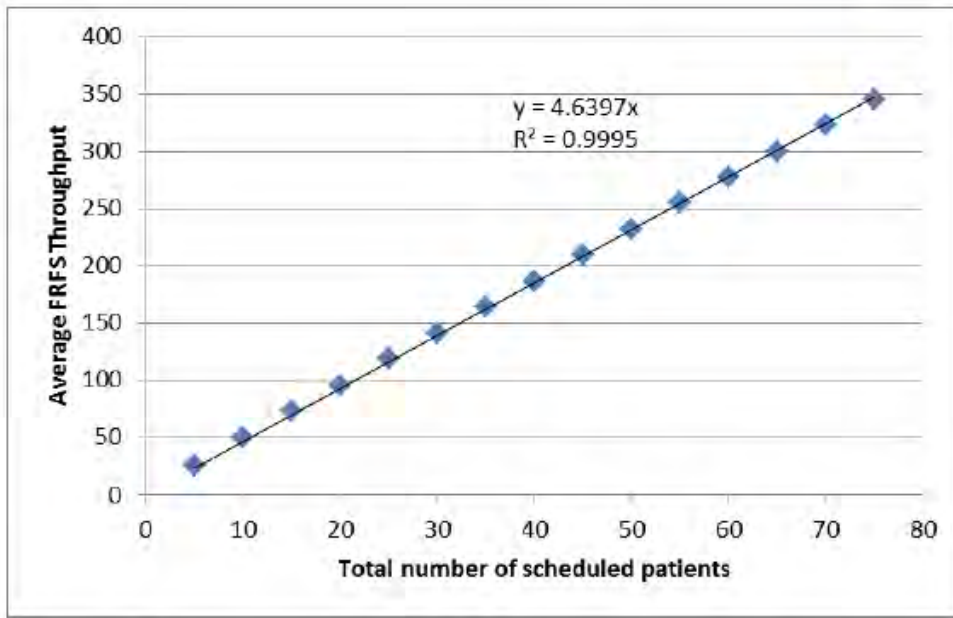


**Figure 13. Average (over 100 random patient sequences) throughput generated by the FRFS algorithm as a function of total number of scheduled patients (deterministic durations).**

A simple linear regression provides a very good fit to these values (with  $R^2=0.995$ ) indicating that, when another 5 patients are added to the sequence, the throughput increases by about 4.64 minutes per patient, on average. Figure 14 “zooms in” on the region between 60 and 75 scheduled patients and adds the average throughput values for the RTSFD (in red) algorithm for comparison.

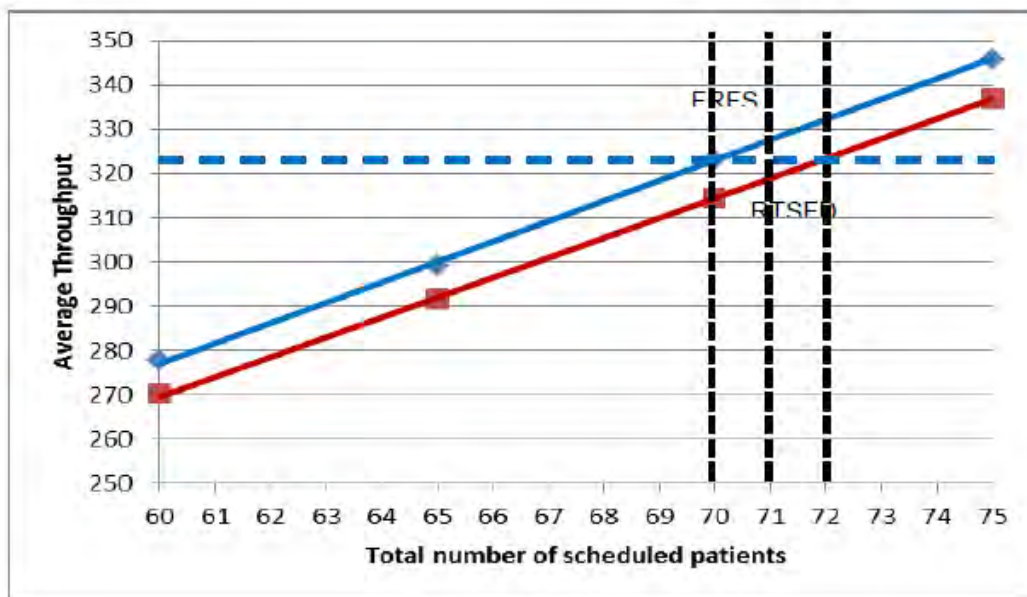




**Figure 14.** Average (over 100 random patient sequences) throughput generated by the FRFS (blue) and RTSFD (red) algorithms as a function of total number of scheduled patients (deterministic durations).

Figure 14 points out that, for example, for  $N=14$  patients in each room (70 scheduled patients in total), moving from FRFS to RTSFD leaves time for 1-2 extra patients per day. Since the curves in Figures 13 and 14 are based on adding 5 patients (1 per room) at-a-time, it is important to analyze a more detailed setting in which patients are added to the sequence one-at-a-time.

Figure 15 shows the average (over 500 random patient sequences) throughput values for FRFS and RTSFD algorithms when the number of patients scheduled changes from 75 (15 patients in each room) to 76 (15 patients in 4 rooms and 16 in the 5<sup>th</sup> room), to 77 (15 patients in 3 rooms, and 16 patients in each of the remaining 2 rooms), to 78 (15 patients in 2 of the rooms, and 16 patients in the remaining 3 rooms), to 79 (15 patients in 1 room, and 16 in each of the remaining 4 rooms), to 80 (16 patients in each room). As Figure 15 indicates, depending on the patient configuration, the use of RTSFD instead of FRFS allows to “inject” between 1 and 3 extra patients within the throughput range generated by FRFS.

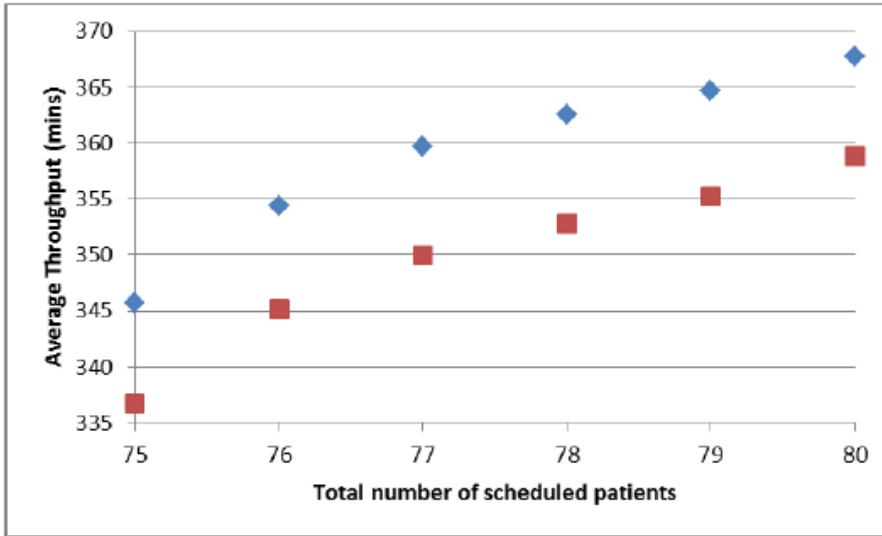


**Figure 15.** Average (over 500 random patient sequences) throughput generated by the FRFS (blue) and RTSFD (red) algorithms as a function of total number of scheduled patients (deterministic durations).

### 2.2.2. RTSFD performance: improving patient sequences.

One important factor in considering potential throughput improvement is optimizing patient sequencing. For the same patient arrival times in each room, simply switching the sequence in which patients are scheduled to arrive can have a measurable impact on the throughput,

and, consequently, on beam utilization. In this Section we report the results of numerical tests in which the improvements in real-time beam allocation are combined with those resulting from using better patient sequences. In our numerical tests, we first looked at the patient sequences with  $N=2$  patients in each room. In particular, we have generated 500 random patient sequences. For each patient sequence, throughput values  $T_{RTSFD}^0$  and  $T_{FRFS}^0$  for RTSFD and FRFS algorithms are calculated. After that, a random permutation of patient sequence in each room is generated, and RTSFD and FRFS are applied again to this permuted patient sequence. Among the results for 50 random permutations, the one with lowest FRFS throughput value ( $T_{FRFS}^b$ ) and the one with the lowest RTSFD throughput value ( $T_{RTSFD}^b$ ) are selected, and the performance gaps  $\mathcal{E}_{RTSFD}^0 = (T_{FRFS}^0 - T_{RTSFD}^0)/T_{FRFS}^0$ ,  $\mathcal{E}_{FRFS}^b = (T_{FRFS}^0 - T_{FRFS}^b)/T_{FRFS}^0$ , and  $\mathcal{E}_{RTSFD}^b = (T_{FRFS}^0 - T_{RTSFD}^b)/T_{FRFS}^0$  are calculated. In other words, the first error term represents an improvement generated by applying RTSFD beam allocation to a random patient schedule, the second term represents an improvement generated by altering patient sequence, and the final one – an improvement generated by combining the two approaches. Table 16 shows the resulting values of these  $\mathcal{E}$  error terms.

	$\mathcal{E}_{RTSFD}^0$	$\mathcal{E}_{FRFS}^b$	$\mathcal{E}_{RTSFD}^b$
Average over 500 patient sequences	2.85%	4.92%	6.23%

**Table 16. Combined performance of RTSFD and improved patient sequence ( $N=2$  patients in each room, deterministic durations).**

As we observe, the average RTSFD contribution of 2.85% can be enhanced to 6.23% by using better patient sequencing. On the other hand, using improved patient sequencing while retaining the FRFS beam allocation approach results in an average improvement of 4.92%. While the contribution of pure patient sequencing appears to be higher, it is in combination of these two approaches that the highest improvement is achieved.

Next, we have applied this approach to a “real-size” problem containing 15 patients in each room. For this larger problem, we have used 50 random patient sequences, and for each patient sequence, 25 different sequencing scenarios. The results are reported in Table 17.

	$\mathcal{E}_{RTSFD}^0$	$\mathcal{E}_{FRFS}^b$	$\mathcal{E}_{RTSFD}^b$
Average over 50 patient sequences	2.62%	3.26%	4.61%

**Table 17. Combined performance of RTSFD and improved patient sequence ( $N=15$  patients in each room, deterministic durations).**

Table 17 illustrates the point that the effectiveness of joint application of effective real-time beam allocation approaches and improved patient sequencing enhances the overall impact on the resulting throughput: RTSFD alone generates an average 2.62% improvement in throughput, while combined with better patient sequencing brings the average improvement to 4.61%.

### 2.3. Stochastic durations.

We have extended our numerical experiments to the setting where the actual durations of the preparations phases and fields for all treatment protocols are random. In our numerical tests we have used the actual data from Dataset 2.

#### 2.3.1. RTSFD vs. RTPIR: fixed patient sequences.

As was done for the setting with deterministic preparation and field times, we first have applied both the RTSFD and RTPIR to 100 randomly generated patient sequences consisting of  $N=1$  patient in each room. As before, by construction of RTPIR algorithm, both algorithms are producing *statistically* identical results in this case. The results are presented in Table 18.

	Throughput RTSFD	Throughput Gap RTPIR	Total Patient Wait RTSFD	Total Patient Wait RTPIR	Max Patient Wait RTSFD	Max Patient Wait RTPIR
Average Gap	0.01512194	0.015565194	0.001212094	0.00188223	-0.046031444	-0.044940352
St.Dev. Gap	0.0088734	0.008853695	0.007162982	0.007187766	0.030105557	0.02992936
Max Gap	0.043998432	0.034632523	0.018419096	0.021117403	0.003177966	0.005498754
Min Gap	-0.000245909	-0.00057117	-0.023968103	-0.011273734	-0.124278677	-0.1328125

**Table 18. Performance of RTSFD and RTPIR for  $N=1$  patient in each treatment room (100 randomly generated patient schedules, random durations).**

Note that, averaged over randomly-generated patient sequence, as compared to FRFS, RTSFD and RTPIR reduce throughput by about 1.5%, with minimum gap of about 0% and maximum gap of around 4.4%. On average, both algorithms reduced total patient wait time by about 0.1%, but increased maximum patient wait time by about 5%. As compared to Table 7, the average throughput gap in the presence of stochastic durations is reduced from 2.9% to 1.5%, and the maximum throughput gap is reduced from 12.9% to about 4.4%. The corresponding distribution of the throughput improvement gap is shown on Figure 19.



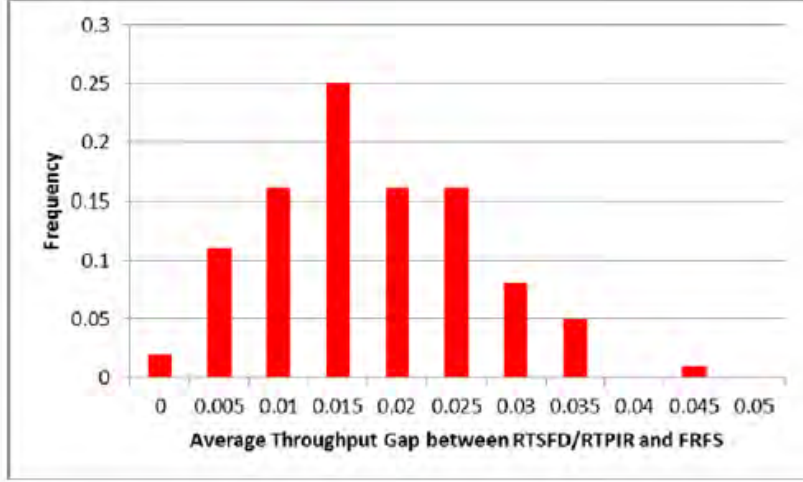


**Figure 19. Distribution of the throughput performance gap for RTSFD and RTPIR algorithms (100 randomly generated patient schedules with  $N=1$  patient in each treatment room, random durations).**

### 2.3.2. Combining RTSFD with improved patient sequencing.

As in case of deterministic durations, the performance of the beam allocation algorithms strongly depends on the selected patient schedule. In order to verify the impact of patient sequencing on the overall throughput reduction, we have conducted the variant of the study described in Section 2.2.2 for  $N=2$  patients in each treatment room. In particular, we have generated 50 random patient sequences, and for each patient sequence, we have applied the adapted version of RTSFD (as described in Section 1.4) and FRFS algorithms to 100 scenarios involving random durations for preparation phases and fields. After that, 10 random permutations of each patient sequence were generated, and the procedure repeated for each permutation. Among the results for 10 random permutations, the one with lowest *expected* FRFS throughput value ( $T_{FRFS}^b$ ) and the one with the lowest *expected* RTSFD throughput value ( $T_{RTSFD}^b$ ) are selected, with expectations calculated over 100 scenarios for each patient sequence. The resulting values of the performance gaps

$\mathcal{E}_{RTSFD}^0 = (T_{FRFS}^0 - T_{RTSFD}^0)/T_{FRFS}^0$ ,  $\mathcal{E}_{FRFS}^b = (T_{FRFS}^0 - T_{FRFS}^b)/T_{FRFS}^0$ , and  $\mathcal{E}_{RTSFD}^b = (T_{FRFS}^0 - T_{RTSFD}^b)/T_{FRFS}^0$  are presented in Table 20.

	$\mathcal{E}_{RTSFD}^0$	$\mathcal{E}_{FRFS}^b$	$\mathcal{E}_{RTSFD}^b$
Average over 50 patient sequence	1.33%	1.97%	3.00%

**Table 20. Combined performance of RTSFD and improved patient sequence ( $N=2$  patients in each room, random durations).**

Similar to the deterministic settings, the RTSFD algorithm and the improved patient sequencing enhance each other's effects on the throughput, resulting in overall 3% throughput improvement, on average.

### **3. Next Steps.**

During the upcoming months, we will focus on the following tasks: 1) creating a working version of the application that relies on the up-to-date patient schedule and real-time events files to produce real-time beam allocation recommendations, 2) fine-tuning the RTSFD algorithm based on actual scheduling and durations data, 3) investigating the performance of real-time beam allocation heuristics that rely only on the knowledge of what patients are currently in treatment rooms, and 4) creating robust patient sequencing recommendations.

## **Walter Reed Remote Proton Radiation Therapy Projects**

### **1). Tissue Inhomogeneity** *Rulon Mayer*

In April, 2012, an article summarizing earlier effort on radiochromic film dosimetry was published (R. Mayer et al., “Enhanced Dosimetry Procedures and Assessment for EBT2 Radiochromic Media”, Medical Physics, 39 pp 2147-2155, 2012)..

A brief summary of those efforts is shown below.

The purpose of this effort was to quantitatively determine an optimum image analysis procedure to mitigate inhomogeneities within the EBT2 film and from scanning to achieve accurate absolute dose measurement deposited by an external radiation therapy beam. Multichannel dosimetry procedures were conceived and quantitatively tested against single and dual channel dosimetry.

A solid water<sup>TM</sup> block was placed on CT imaging and treatment tables in a configuration that avoids bulky compressive devices. CT markers helped register the CT to the treatment plan and the radiation dose distribution from the radiochromic film. The CT images were digitally rotated and resampled to match the spatial resolution of the scanned dosimetric distribution and treatment plan. The ECLIPSE treatment plan planes were digitally translated using CT markers. A 6 MV photon beam, conforming to the treatment plan, irradiated the EBT2 film sandwiched between solid water<sup>TM</sup> slabs. The exposed radiochromic film images were rotated and translated to the CT images using coincident markers in the CT image and “tattoos” marked on the radiochromic film.

The exposed radiochromic film grey-levels from a flatbed scanner were converted to dose using calibration films. The test dose distribution was scanned and averaged to reduce temporal noise. This study generated dose distributions using the red and green channel alone, ratios of red to blue channel and of the green to blue channel, a “Hybrid” approach combining the green to blue ratio for higher doses with the red to blue ratio (<80 cGy), multichannel averaging and optimized autonomous multichannel correction.

Single channel, multichannel, and channel ratio methods for processing the exposed radiochromic film were compared to the treatment plan via gamma analysis. The ellipsoidal decision surface was defined by its axes of 3% of the maximum dose, and 3 mm in the horizontal and vertical directions.

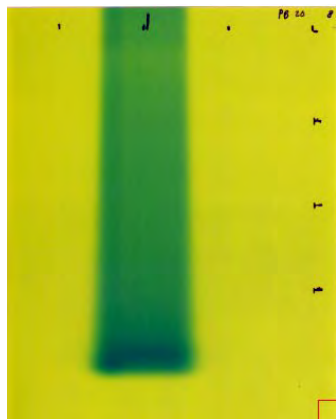
In summary this study described, developed and tested new processing methods for reducing inaccuracies in absolute dose determination due to inhomogeneities within the film and from scanning. The multichannel dosimetry procedures provided excellent agreement with calculation of the dose distribution as determined by the gamma analysis. The green channel mostly performed as well or better than the red channel. The “Hybrid” approach achieved a high level performance. Also, new registration procedures were developed and tested to aid comparing calculated and experimentally determined dose distributions. This study found better performance for optimized multichannel following averaging of all color channels (by reducing temporal noise that severely degraded the blue channel). This methodology avoids cumbersome, registered correction matrices. Novel registration and digital rotation of CT images enabled better, simple contact between the radiochromic film and phantom.

The effort this Spring, 2012 focused on testing radiation dosimetric distribution deposited by protons exposing a radiochromic film sandwiched between slabs of solid water. There is currently controversial issue regarding the sensitivity of the radiochromic film and protons, especially near the Bragg Peak. At the Bragg Peak, protons slow down precipitously within a short distance (smaller than the width of the sensitive layer within the radiochromic film) reducing the sensitivity of the film according to many (but not all reports). This study will examine and attempt to compensate for the diminished sensitivity of the radiochromic film.

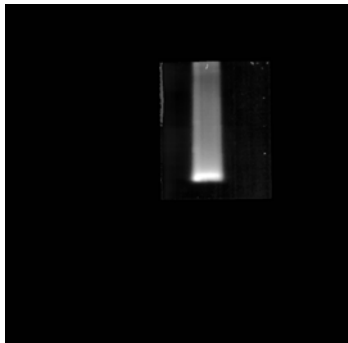
The telemedicine issues involving communication between Walter Reed NMMC and University of Pennsylvania were resolved this Spring, 2012. ECLIPSE treatment planning located at University of Pennsylvania server was conducted remotely in Bethesda. To achieve “purer” Bragg peaks, the Pencil Beam at the University of Pennsylvania was used instead of the double scattered beams. ECLIPSE currently does not permit planning to a fixed point, except at the isocenter. Due to limited time constraints for proton research, the solid water phantom was positioned at a fixed source to phantom surface distance. Such an arrangement required creating a thin gross tumor volume for treatment planning purposes. The finite thickness required for treatment planning volume implies energetically (and spatially) broadened Bragg peak. To achieve variable range, the proton energy was varied to generate six beams with ranges of 8 cm up to 20 cm. In addition three spread out Bragg peaks with ranges of 10 and 12.5 cm and modulated by 2.5 to 5 cm were created by the ECLIPSE system. System parameters to generate the nine beams were transported to the Pencil beam.

Subsequently, nine protons beams (six “pure” Bragg peaks, three spread out Bragg peaks) derived from the remote ECLIPSE planning system exposed the radiochromic films. The procedure for registering and comparing the dose distribution from the radiochromic films and treatment plans were described in the published Medical Physics article

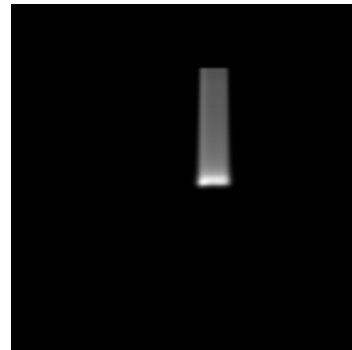
**Proton Exposed, Radiochromic film, 20 cm range**



**Multichannel Optimized Dose Distribution, Registered, Proton 20 cm Range**



**ECLIPSE plan, Registered, Proton 20 cm Range**

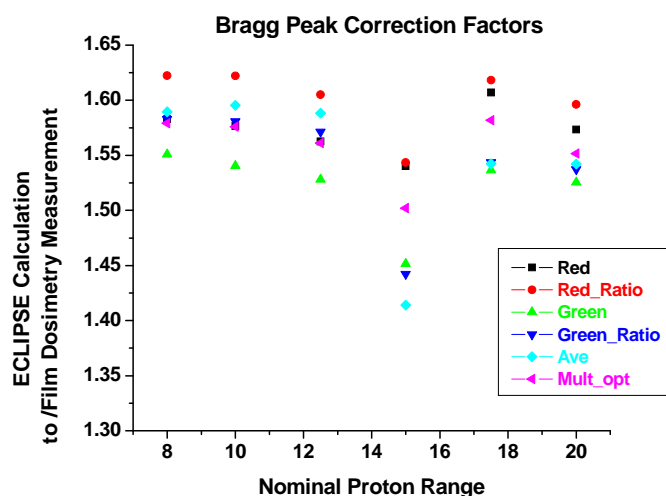


This summary describes recent effort for examining the proton distribution in a uniform solid for single energy and spread out Bragg Peaks (SOBP). In addition, this effort compares the method described previously to methods derived from another group (Devic, Med Phys. 2012) , namely a three degree polynomial fit. To further test possible approaches and for the sake of completeness, a four degree

polynomial fit was also tested. Unlike Devic, 2012, this analysis examined both the simple Bragg peak and the Spread Out Bragg peak. In addition, it applied gamma analysis to an area and to a number of dose distributions from a variety of ranges within the solid water. This effort attempts to use radiochromic film for generate absolute dosimetry, not only relative dosimetry. Radiochromic film suffers especially in high LET due to the finite thickness of the dosimetric media. Polynomial fits fail to accommodate the high does regions, unlike the shifted profile correction method suggested in this note.

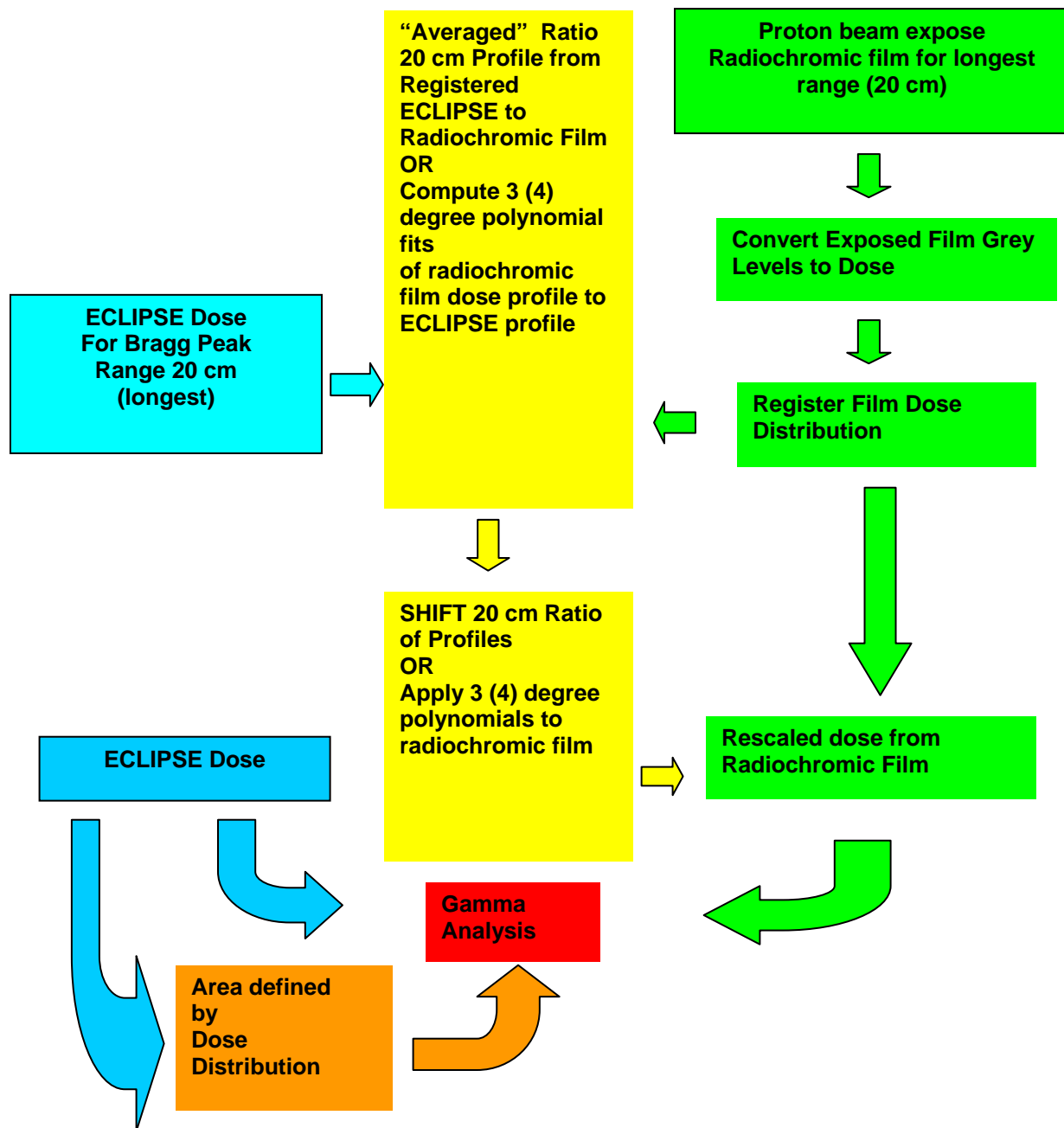
These effort will support further efforts involving heterogeneous materials. A heterogeneous phantom (air, cork, higher density plastic) has been constructed and will soon be assembled. The heterogeneous phantom will be scanned and x-ray and proton treatment plans will be generated for application. The approaches and code described in this missive will be applied to the heterogeneous phantom.

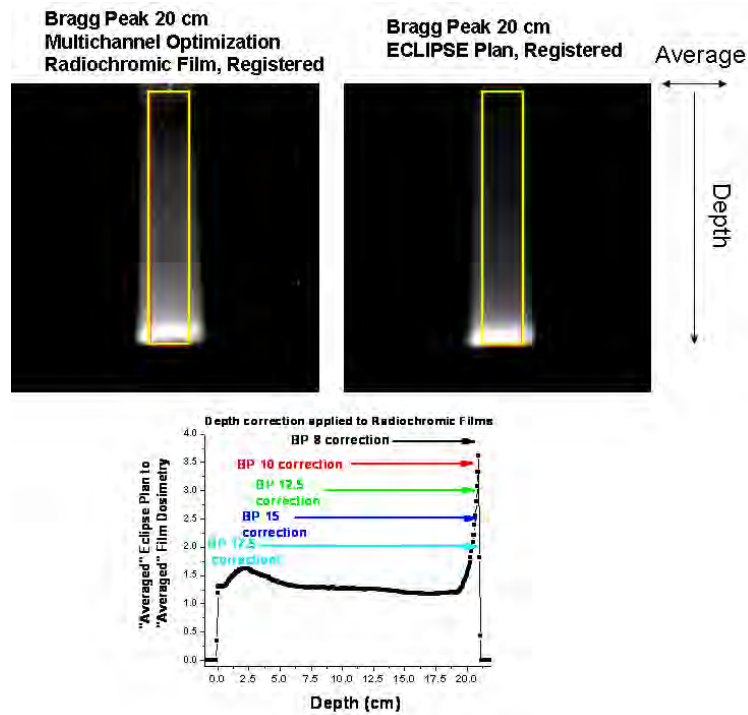
This effort generates a correction for proton depth dose deposited in a solid water phantom and using radiochromic film dosimetry. This is a summary that examines “single energy” Bragg peaks and spread out Bragg peak dose distribution. It is (and has) been noted that protons slow near the end of the range and have high LET. The relative insensitivity of radiochromic film has been observed and confirmed in this study. However, it is noted that the sensitivity of the film for protons within the Bragg peak seems to be a common feature for a variety of proton energies. The figure below plots the average relative response (ECLIPSE treatment plan to measured radiochromic film dose within 90% of the peak. The figure shows the correction using a variety of processing methods developed and discussed earlier (Mayer et al, 2012).



To correct for the entire field, the overall processing scheme was developed and shown below. It is hypothesized that the entire correction is due to variable radiochromic film response as a function of depth due to proton LET variations. It should be noted that the films were calibrated using 6 MV photons with the plane of the film perpendicular to the beam. Earlier efforts examined normalized profiles but this effort focuses on absolute dosimetry.







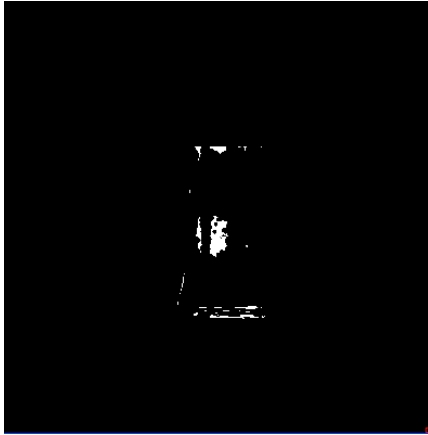
The correction factor is computed by averaging over the horizontal direction within a relatively uniform area (away from beam edges). The correction is ratio of the ECLIPSE computed dose to measured film response. In the example, only the multichannel optimized algorithm is employed in this analysis.

The correction factor increases near the Bragg peak. This increase is due to the increased LET and resulting reduced sensitivity to proton dose deposition by the radiochromic film. In addition, the sharp peak in the correction at the very end of the Bragg peak is due to a small misregistration error, where the LET is at its maximum.

The source for the correction factor was derived from the dose distribution deposited by the proton beam having a range of 20 cm. Correction factors for the other beams having shorter ranges (8, 10, 12.5, 15, and 17.5 cm) were generated by shifting the correction by a variable amount and searching for the minimum number of gamma exceedance (3% dose, 3 mm elliptical decision surface). The shifts are also schematically shown in the plot of the correction factor.

Number of exceedances beyond the gamma analysis ellipse (3% of maximum dose, 3 mm) is a measure of the agreement between ECLIPSE plan and film dosimetry. Figure shown below, displays the number of exceedances for the proton Bragg Peak having ranges 12.5 cm and 20 cm. The film dosimetry was corrected using the correction factors from the Bragg Peak having a range of 20 cm.

**Bragg Peak, Range 12.5 cm**



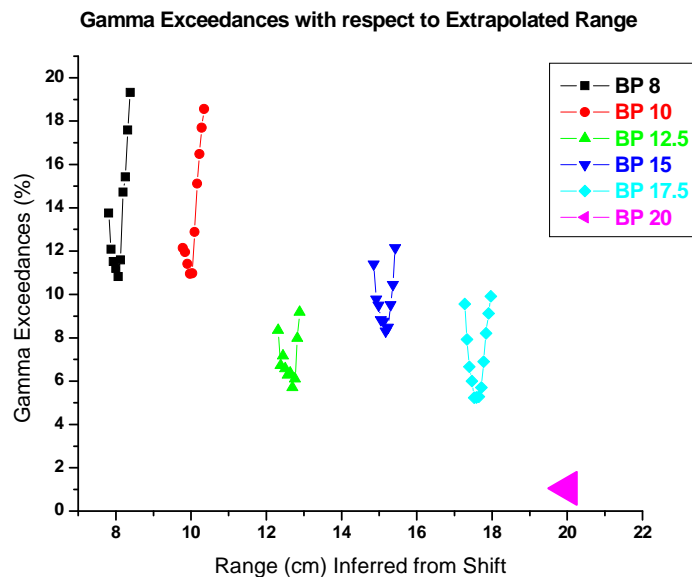
**Bragg Peak, Range 20 cm**



Gamma

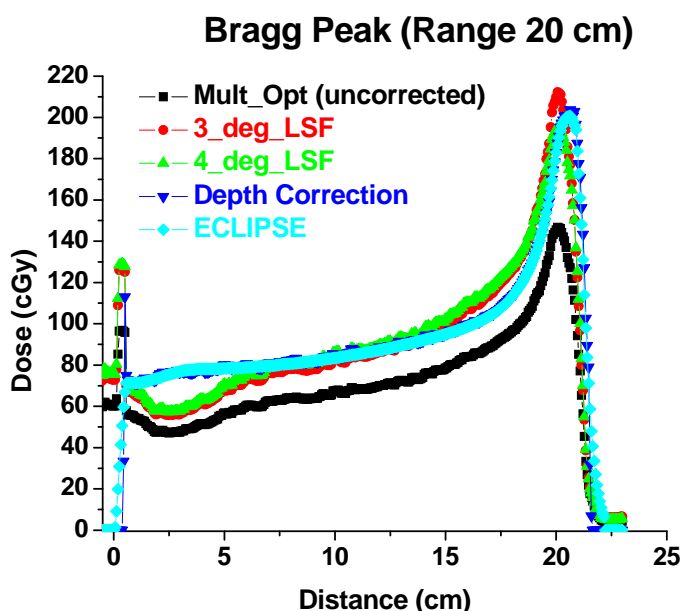
Exceedances (3% Maximum dose, 3 mm), Corrected Multichannel Optimized

Below is the plot of percent of gamma exceedances for variable shifts. As shown in the figure, there is a sharp minimum in the exceedances that correspond (within less than a millimeter) the expected shift based on the nominal ranges. The minimum in the curves falls within 0.5 mm of the expected shift.

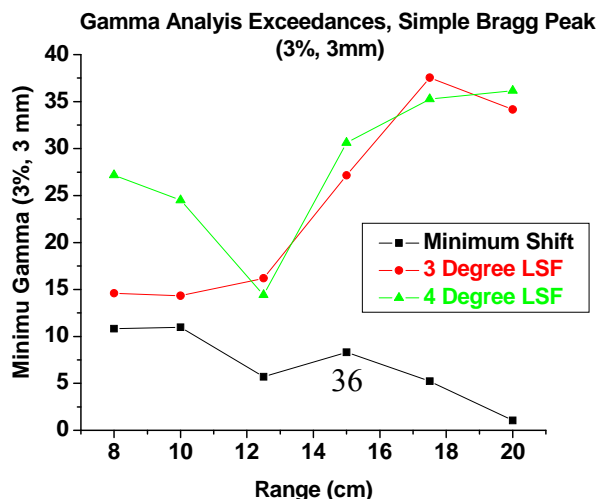


The lowest number of exceedances occurs with the Bragg peak corresponding 20 cm, or zero shift. More exceedances occur for protons with Bragg peaks that lie further away from 20 cm or maximum range used in this study.

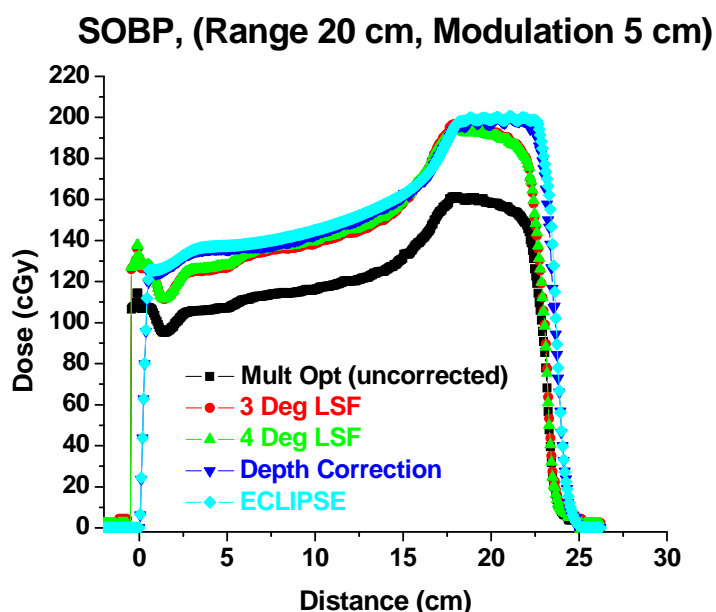
Devic, 2012 examined applying a polynomial least square fit to proton depth profiles. Devic only applied a three degree polynomial to the profile and did not apply it to an area exposed to protons and applied it to single energy Bragg peaks.. This study compared ECLIPSE and processed radiochromic film vertical profiles generated by averaging in the horizontal direction. Both three and four degree polynomials were fit the profiles and the coefficients were applied to every pixel in the processed radiochromic film. The figure below shows the calculated ECLIPSE dose for protons the corrected radiochromic films using fitted 3 and 4 degree polynomial coefficients,, the scaled profile, and uncorrected radiochromic film dose distribution. The best match to the calculated ECLIPSE profile uses the scaled depth dose approach. Fitting functions of the data does not account for the discrepancies in the high LET region (or higher energy portion) of the Bragg peak.



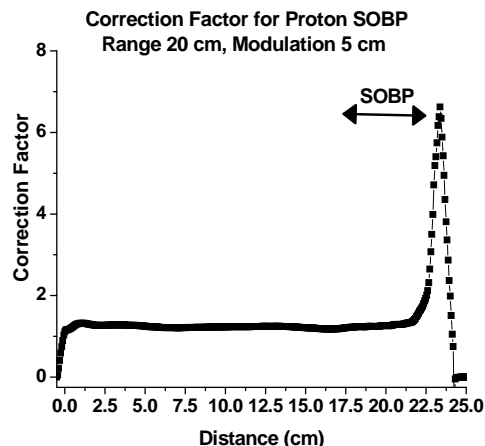
The figure shown below directly compares the depth dose scaling approach with the polynomial fit. The shifted depth dose approach yields smaller number exceedances and hence greater agreement with the ECLIPSE dose distribution over an extended area. There seems to be little difference between using 3 or 4 degrees for the polynomial fit over all ranges. The analysis uses 3% of the maximum dose and 3 mm in horizontal and vertical directions as the parameters in the gamma analysis.



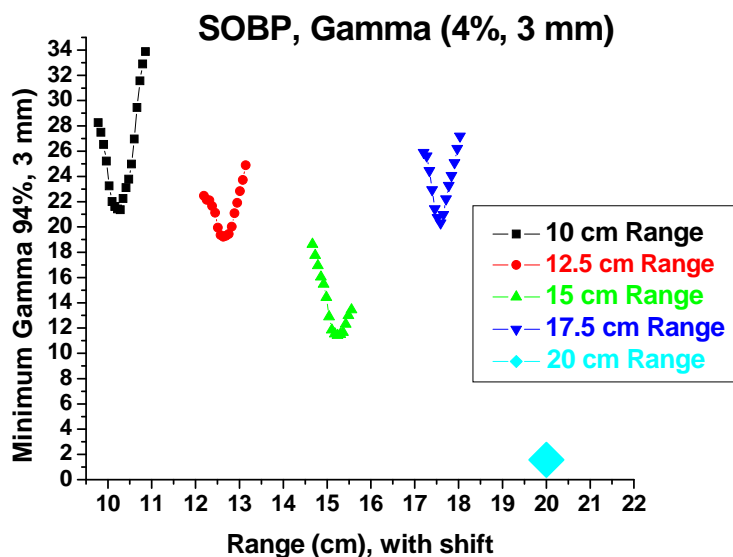
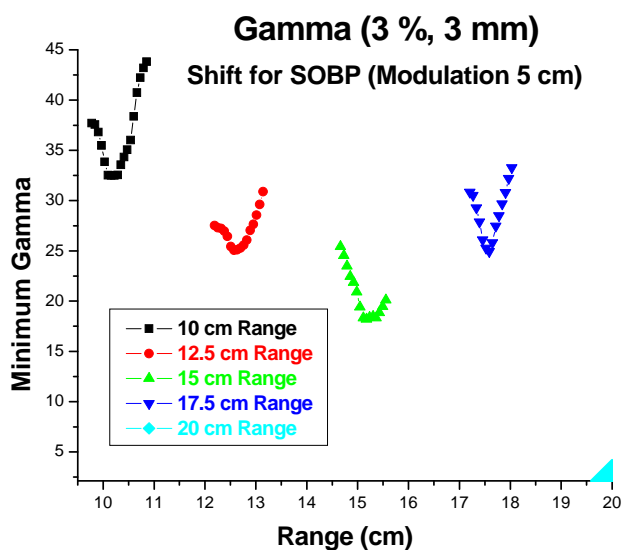
This analysis has been extended to protons with modulation or having Spread Out Bragg Peak. The ECLIPSE depth profile, 3 and 4 degree polynomial fits applied to the processed radiochromic film, the depth profile correction and uncorrected profiles for the protons having a range of 20 cm, and modulated by 5 cm. are displayed below. The high LET range or high energy part of the SOBP shows significant deviations. The relative capacity of the profile is enhanced for SOBP relative to single energy Bragg peaks.



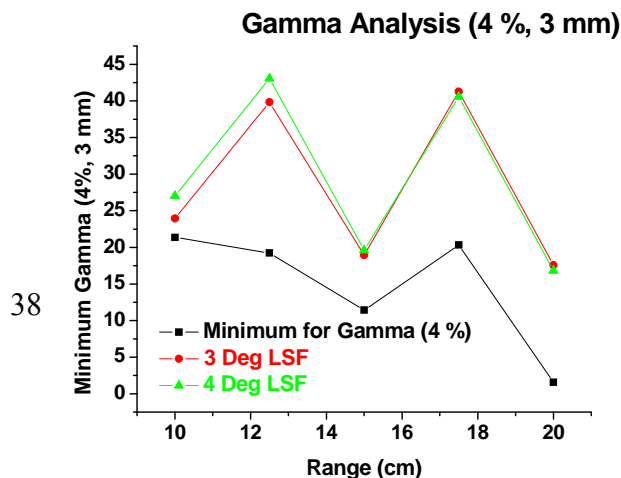
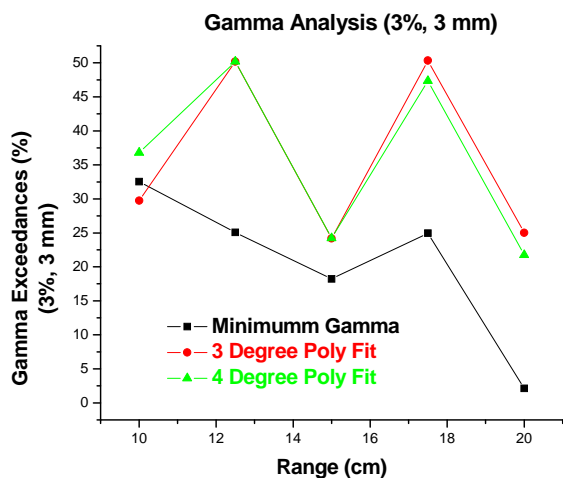
The correction factor for the proton SOBP with range of 20 cm and modulation 5 cm was computed by taking the ratio of the ECLIPSE dose with the radiochromic film dose computed using multichannel optimization. Again, the correction factor is generally flat until the end of the range. It appears that numerically this correction factor follows the expected LET. The slowing protons deposit their energy over a short distance. The correction factor is relatively flat over the SOBP due to contributions from the contributing higher energy Bragg peak protons that still have high energy and low LET.



The shifted profiles for the SOBP are shown below for two sets of Gamma analysis parameters (3 %, 3 mm) and (4%, 3 mm). The minimum in these curves can depart as much as 2 mm from the expected shift. The relative number of exceedances is greater than that found for the single energy Bragg peaks. The figures shown below for the SOBP



The figures shown below for the SOBP directly compares the depth dose scaling approach with the polynomial fit. The shifted depth dose approach yields smaller number exceedances and hence greater agreement with the ECLIPSE dose distribution over an extended area. There seems to be little difference between using 3 or 4 degrees for the polynomial fit over all ranges. The analysis uses 3% and 4% of the maximum dose and 3 mm in horizontal and vertical directions as the parameters in the gamma analysis. In all cases the depth dose correction provided a better fit to the ECLIPSE treatment plan.



The shifted depth correction method achieves better agreement for the simple Bragg peak relative to the application to the spread out Bragg Peak. Nevertheless, the depth correction should be improved, especially for SOPB.

## 2). Organ motion

*Jessica Sheehan*

A phantom lung has been designed to study the effects of organ motion during proton radiation treatment. This study will allow researchers to determine the amount of radiation a tumor and other parts of the lung receive for comparison to the radiation treatment. The accuracy of proton radiation dose prediction can be determined from this study. Several iterations of this design have occurred to the complexity of mimicking both lung motion and tissue.

### **Initial Dynamic Lung Phantom Design**

The first design dynamic lung phantom was to be encased in a Plexiglas structure to restrict the lung motion slightly to mimic a human chest cavity, **Error! Reference source not found..** The lung will be built at Walter Reed National Military Medical Center (WRNMMC), and tested there as well as the University of Pennsylvania. The lung material will be low density polyethylene, density  $\sim 0.91 \text{ g/cm}^3$ , matching that of lung tissue. The lungs will be made at WRNMMC using a heat sealer to customize the shape, and permit the addition of gafchromic and tumors. The gafchromic will be used to measure the amount of radiation that is exposed to the tumor and various parts of the lungs. The lungs are built for the easy addition and removal of the gafchromic and tumors, and for repeated use of a single set of lungs. The tubing connected to the lungs will consists of several control

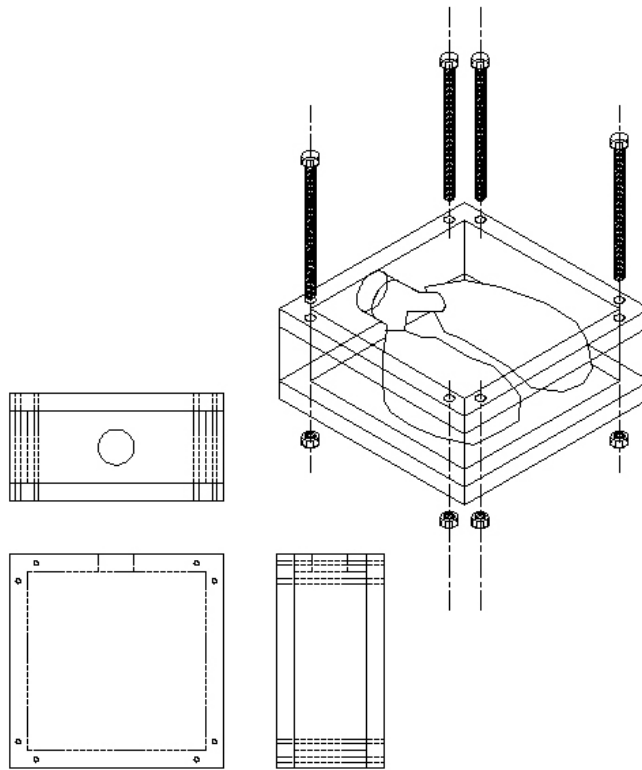


**Figure 1: Schematic of First Dynamic Lung Phantom Design**

valves that will allow for both homogeneous and non-homogenous breathing to be simulated. The pump will be connected to a relay with timer functions to create the breathing cycles. The pressure of each lung is measured separately to ensure no leaks have occurred, as well as the air flow rate. After examining the predictability of dosing with motion, avenues of tracking this motion to modify the dosing to increase accuracy will be reviewed.

### **Modified Dynamic Lung Phantom Design**

The initial prototype of the phantom lung, design outlined in the previous section, was constructed to test feasibility. Although preliminary testing shows the prototype works as theorized, enhancements to the design are desired for robustness of the device. The material used to represent the lung tissues, low density polyethylene (LDPE), was specifically selected to match density characteristics of lung tissue for imaging purposes. However, at thickness of 0.006 inches the material has an undesired rigidity that interferes with lung motion. In addition, discussions amongst the research team have introduced refinement of the phantom lung to be more comprehensive. Specifically the phantom lung would include more anatomic features such as artificial lung tissue that is less rigid, internal lung structure, and inclusion of the organs' influence surrounding the lungs. These additions will be accomplished through a refinement in the current design with reducing the thickness of the artificial lung tissues to limit rigidity,



including inner lung tissue structure represented by a core sponge structure, and addition of water surrounding the lungs in the artificial chest cavity to simulate the influence of neighboring organs.

A reduced thickness LDPE was purchased and tested with positive results that the rigidity issues found with the previous material are mitigated. However, in creating the lung structure seams are necessary and introduce additional rigidity issues. The issue is complicated since the seams are necessary to provide anatomical similitude, thus limiting them to improve stiffness is problematic. The seams are currently created through heated plastic sealer. To produce a more anatomical structure, fabricating seams using a water proof epoxy will be tested to determine if this produces less rigidity issues. Thus, with thinner LDPE and multiple methods to create the lung structure a more anatomic model can be created.

Additional anatomical features are desired to create a robust model and working phantom lung. Inclusion of an internal structure using cellulose sponges molded into a lung shape would not only represent the internal structure, but could aide in creating lobe shapes closer to human lung lobes. Figure 2 shows the schematic of the cellulose sponge enclosed in the LDPE with an air tube attached. Cellulose sponges have a lower density than found in lung tissue. Thus, imagining and dosing would have to be corrected for this. Due to this negative attribute of the addition of the internal lung structure, two phantoms will be simultaneously developed and tested. If both phantoms have good motion and structure, then further testing and comparison between the two phantoms will be conducted to determine the superior design.

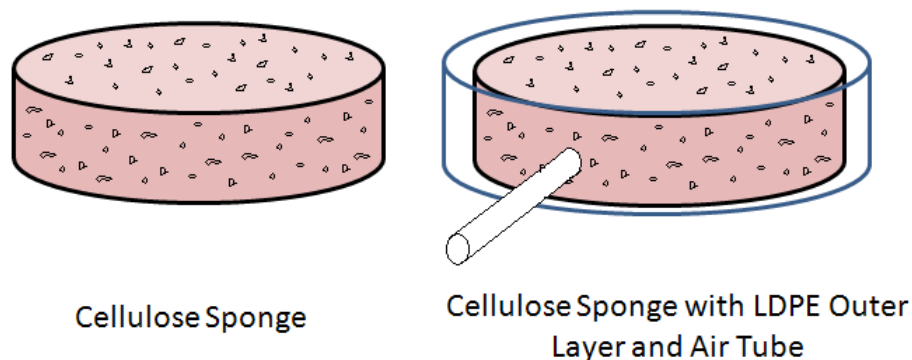


**Figure 2: Schematic of Internal Lung Structure Adaptation**

The third refinement to the designed required the representation of the surrounding organs' influence on the motion of the phantom lung. This is accomplished by filling the chest cavity, described in previous progress report, with water to represent the forces generated by the presence of the additional organs. Figure 3 shows the enlarged artificial chest cavity with thru hole for air tubes being repositioned to the upper portion of the box to limit leaking issues. The addition of water improves the similitude to the anatomical structure since the density of water is a known match for most biological tissues.

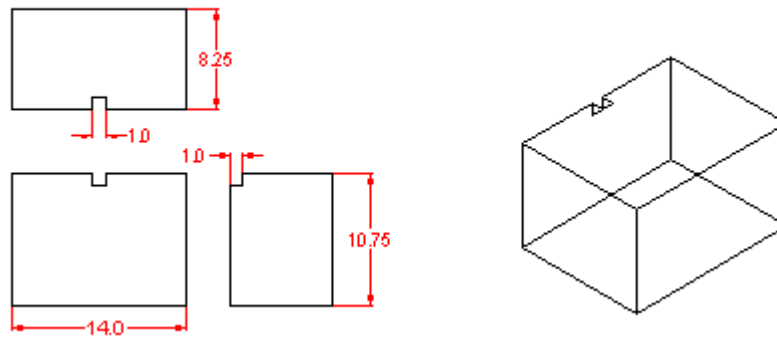


**Figure 3: Artificial Chest Cavity**

### **Results from Modifications of Design**

The two modified phantoms, Figure 4 and Figure 5, were constructed to vet the refined design parameters. The various epoxies tested proved insufficient to air and water seal the lungs given the LDPE surface, resulting either in inevitable breakdown of the flexible seal or cracking of a rigid one. Several epoxies were vetted with no positive results, and some discussion of other methods yield little viable solutions. Figure 4 shows a heat sealed lung set, fulfilling the air and water resistant seal. However, the desired shape is difficult to produce. Figure 5 shows the cellulose sponge material enclosed in the LPDE, also heat sealed in this case. The internal structure makes it extremely difficult to create a good seal close to the sponge. In addition, it is even more apparent how this design



**Figure 4: Modified Dynamic Phantom Lung**



**Figure 5: Modified Dynamic Phantom Lung with Internal Sponge Structure**

would limit the tumor motion when it would be added. Further discussion of the poor match of the sponge material to lung tissue and the mitigation of lung motion has concluded that this is not an advantageous design addition. However, since the proper lung tissue similitude would be desired discussions have lead to a new method of including the internal structure. Figure 6 shows the tumor structure that would be used to include the internal lung tissue without mitigating the movement. In addition, cork can be used to represent the internal lung tissue which properly matches the properties which was not viable previously due to rigidity.

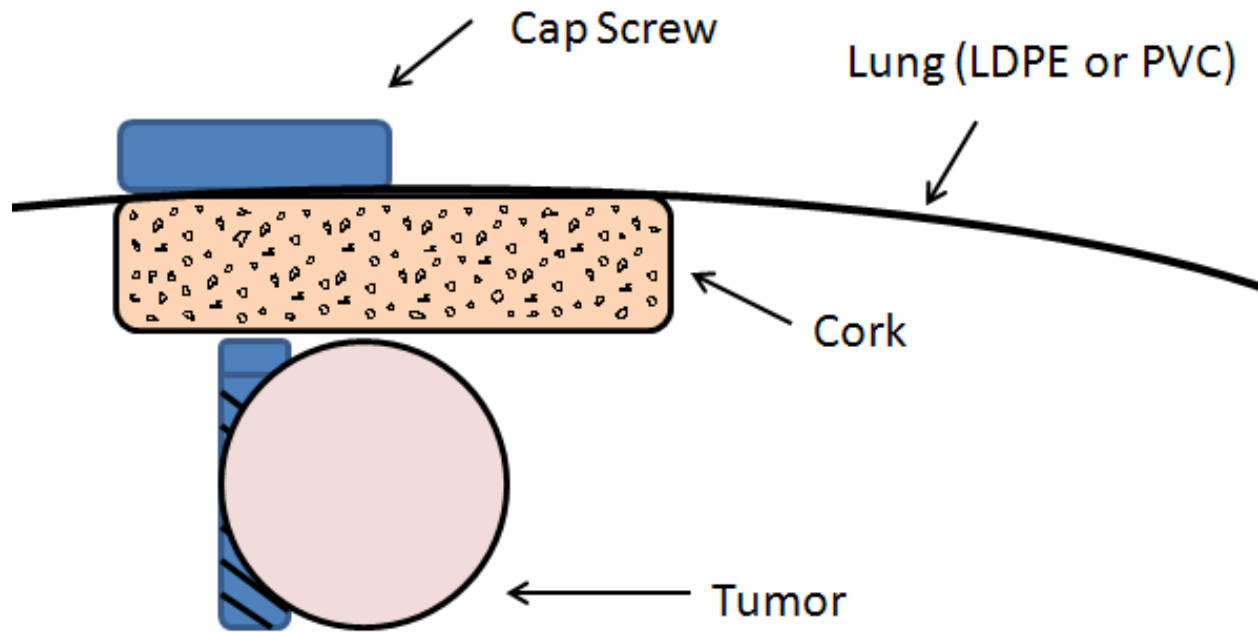


**Figure 6: Tumor Structure**

Since heat sealing did show promising results with successful lung sets being constructed, further improvement on this method is being explored. Since the resources are limited to internal improve upon this method, companies that could custom make the lung structures were researched. After vetting several companies, Jet Creations (locally based) was found to be able to create the shape, size, and easily custom the inflatable to the specific needs of the project. The material strictly used by this company is child-safe PVC, with thickness that can be varied for the project's needs. Figure 7 shows an educational set of lungs the company fabricated revealing their ease in creating air and water tight lung structures with high similitude to human anatomy. Due to the company's expertise in creating such structures it seems likely that the resultant product will work well for the research needs of the project. Further discussion of the exact custom design desired is ongoing, but will mostly likely yield in a purchase of a set of lungs.



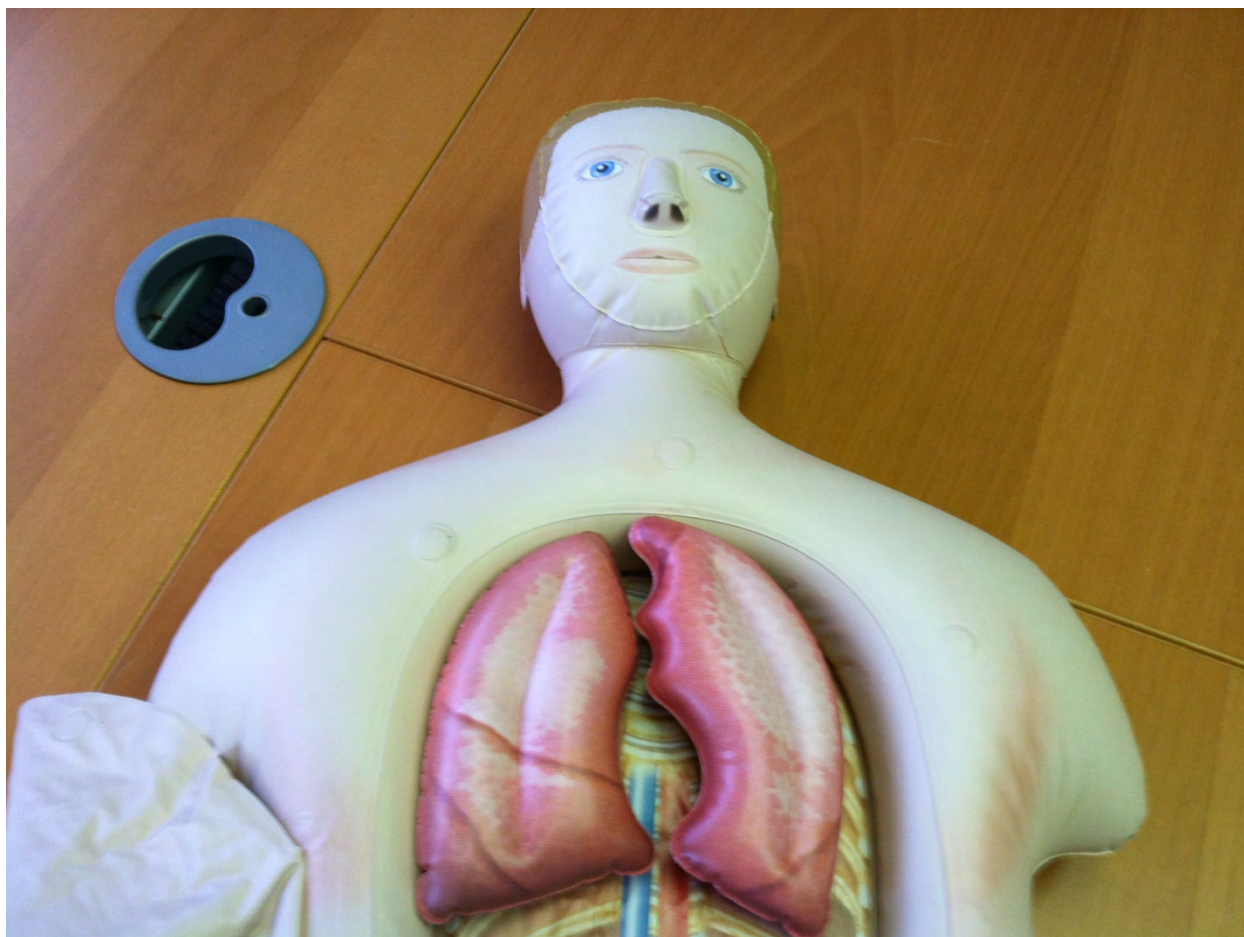


**Figure 7: Educational Inflatable Lung Set (Not to Anatomical Scale)**

### **Stationary Heterogeneous Lung Phantom**

In conjunction with ongoing efforts to create the complex dynamic lung phantom, design and construction of a stationary heterogeneous lung phantom was conducted. Investigation of the predictive models of radiation dosing of the heterogeneous tissue present in the human lung yielded a need for a heterogeneous phantom lung. Figure 8 shows one of four plates comprising the stationary heterogeneous lung phantom. The top and bottom of the four plates is used as a cover for the two internal plates possessing the three one-inch holes. These holes are used to create the heterogeneous tissues structure for testing, with each hole being filled with varying density materials from the main structure. Figure 9 shows an image of two top plates and one internal plate. Each plate is made from acrylic with a density of  $1.18 \text{ g/cm}^3$ , with the holes being filled with: PEEK (density  $1.32 \text{ g/cm}^3$ ), cork (density  $0.24 \text{ g/cm}^3$ ), and air (density  $0.0012 \text{ g/cm}^3$ ). The stationary heterogeneous lung phantom is currently being used in ongoing research.

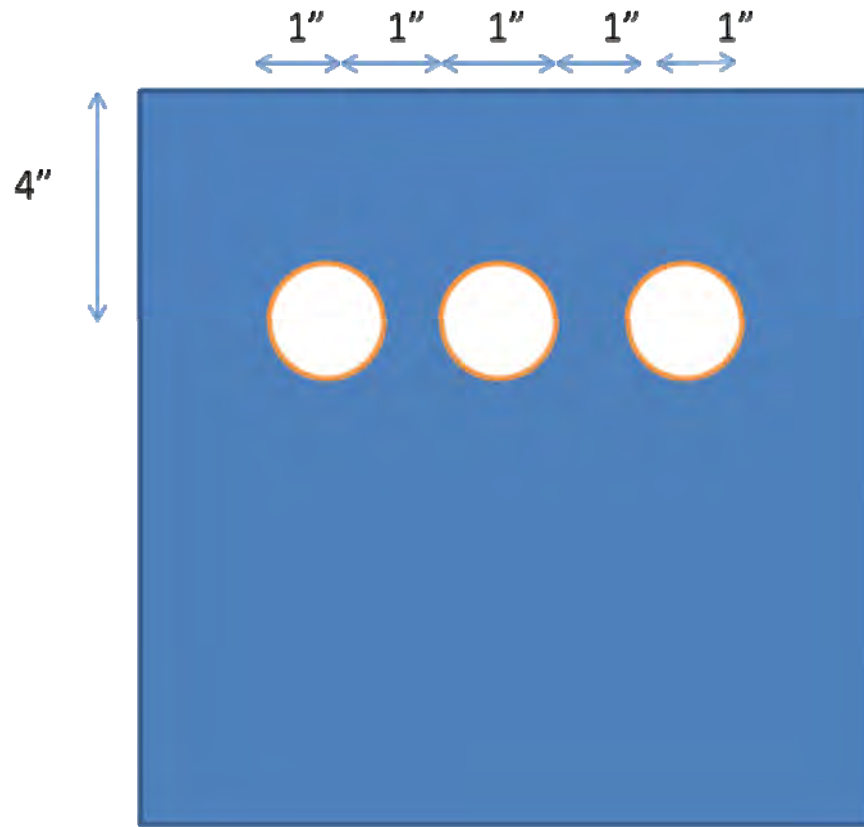


**Figure 8: Stationary Lung Phantom Drawing-Internal Plate**



**Figure 9: Picture of Disassembled Stationary Lung Phantom**

3). Telemedicine update  
*Arnaud Belard*

a). The Tandberg 1700 MXP units transferred to the Walter Reed National Military Medical Center (WRNMMC) and configured on the NNMCC VLAN were initially not being supported by the Information Technology Department (ITD), following guidance by the Joint Task Force (JTF) Chief Information Officer (CIO). At hand was the issue of the units not being owned by WRNMMC but by the Henry M. Jackson Foundation for the Advancement of Military Medicine.

The Program made the case that these units were purchased and deployed as part of a comprehensive remote proton radiotherapy treatment planning solution and that the design, testing and deployment of this system is one of the deliverables of our \$43 million, seven-year on-going, research effort linking the Radiation Oncology departments of the University of Pennsylvania and the Walter Reed Army Medical Center (now the Walter Reed National Military Medical Center).

We further articulated that this solution relied on our physicians' ability to conduct ad-hoc videoconference calls with their counterpart(s) at the Hospital of the University of Pennsylvania, should problems occur during the planning of treatments and/or during the setup of patients (i.e. minutes before radiation treatment is to be delivered). While these units were indeed owned by the Henry M. Jackson Foundation, we argued they were purchased via a DoD research grant to fulfill a patient-care objective at this MTF. In addition, the units were JITC-certified, patched to the latest version and under a maintenance contract until DEC 2013 (after which they will be donated to WRNMMC).

The JTF CIO instructed his team to look into the matter. Following numerous exchanges, an agreement was reached to support these units. Realizing this telemedicine solution is integral to the care of cancer patients receiving proton radiotherapy, the ITD agreed to troubleshoot connectivity issues as they arise, to include gatekeeper/gateway registration with USAMITC.

During the course of the summer, our ability to connect was hindered. Walter Reed Bethesda experienced a faulty network card, preventing ISDN calls from the outside (using the 210.250.xxxx prefix). This particular issue was eventually addressed and we now have the ability to once again conduct audio-video teleconferences with outside institutions.

Robust connectivity with the University of Pennsylvania's Radiation Oncology Department remains elusive however (audio but no video incoming to UPenn). We continue to suspect that the problem lies with how the Polycom RMX bridge handles incoming calls from Walter Reed Bethesda. The issue is still being investigated.

#### b) Remote treatment planning

In December, we were informed by the University of Pennsylvania Health System (UPHS) that the Junos client (Juniper) would replace the CITRIX Access Gateway (CAG) for VPN access. This decision to switch clients was communicated to us abruptly (i.e. 24-hour shutoff window). With the help of the RadOnc IT staff, we made the case to UPHS that, Junos not being approved for deployment on a DoD network, we needed an extension of the CITRIX client. We were granted that extension until MAR 01 2012 (three months).

We quickly identified that Junos was not approved for deployment on a DoD network ; however, the Juniper Net Connect client, a suitable alternative as far as UPHS is concerned, was. Reaching to the JTF-ITD, we quickly worked on getting this solution up-and-running, before the termination date of the CAG (FEB 29 2012).

Initial requests to have the client installed on all provider PCs, to include physicians, medical physicists and dosimetrists, was denied. Our program floated the idea of having a single PC, to be placed on the DMZ, configured as a 'jump box', from which providers could launch the Juniper Net Connect Client and remotely access the proton treatment planning package at the University of Pennsylvania. The approach was approved and subsequently configured over the course of several weeks.

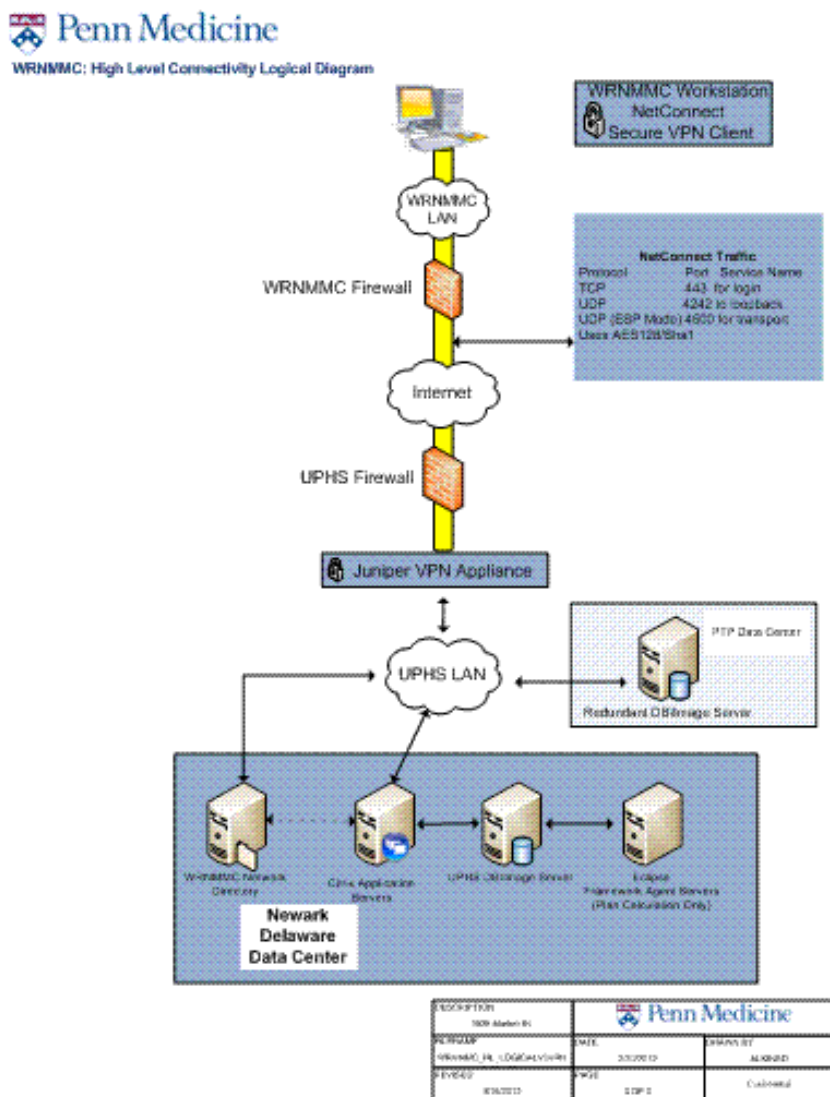
While the solution does work, it is sub-optimal. Not only does this approach require users to work from a unique location when planning a proton plan remotely, the solution does not integrate within our existing infrastructure since the 'jump box' does not touch the network (i.e. any treatment data has to be burned on a CD and manually transferred) and limits itself to a single user at a time. We will keep engaging the JTF-ITD with the hope that the current system, a downgrade from what we previously had with the CAG, will serve as a basis for future upgrades.

We continue to use the limited solution pushed for, but supported by, the JTF-ITD (i.e. single machine residing on the DMZ). This a major downgrade from the solution we had at the Walter Reed Army Medical Center (CITRIX-powered solution residing on all providers' PCs, themselves paired with audio-

videoconferencing units). We hope to re-visit the minimalist approach proposed to us by the JTF-ITD once the migration to the JMED network is complete.

Dr. Mayer (research scientist) and Ms. Wan (medical physicist) have been using this system repeatedly during this quarter for both research and training, and have experienced intermittent disconnections. As of now, the stability of the system is therefore in question, with flawless connectivity on some days and inabilities to connect on others. We suspect our testing and use of the system have this quarter suffered from the migration of the NMED to the JMED (i.e. occasional network slowdowns and/or drops).

The logical connectivity diagram below highlights the current telemedicine setup (including the Juniper VPN client).





c). Anticipated use of system for actual treatment planning

While not an effort conducted on this research grant, the first of our Cooperative Research and Development Agreements (CRADA) was signed by the University of Pennsylvania the third week of December and is now undergoing final review at WRNMMC; we hope ADM Stocks (Commanding Officer, NSA-Bethesda) will sign this agreement during the first few weeks of the new year.

This first CRADA will serve as a template for 16 subsequent submissions (disease-site specific clinical trials looking at toxicity and quality-of-life for proton radiotherapy treatments). Our telemedicine solution will be supporting this effort.

The operational use of the telemedicine system is contingent upon the approval of our clinical trials (a parallel, and complementary, effort to this cooperative-agreement). Of a planned twelve trials, three have been approved:

i) Proton Radiation for Low-Grade Gliomas

ii) A Trial of Proton Radiation Therapy Using Standard Fractionation for Low-Risk Adenocarcinoma of the Prostate

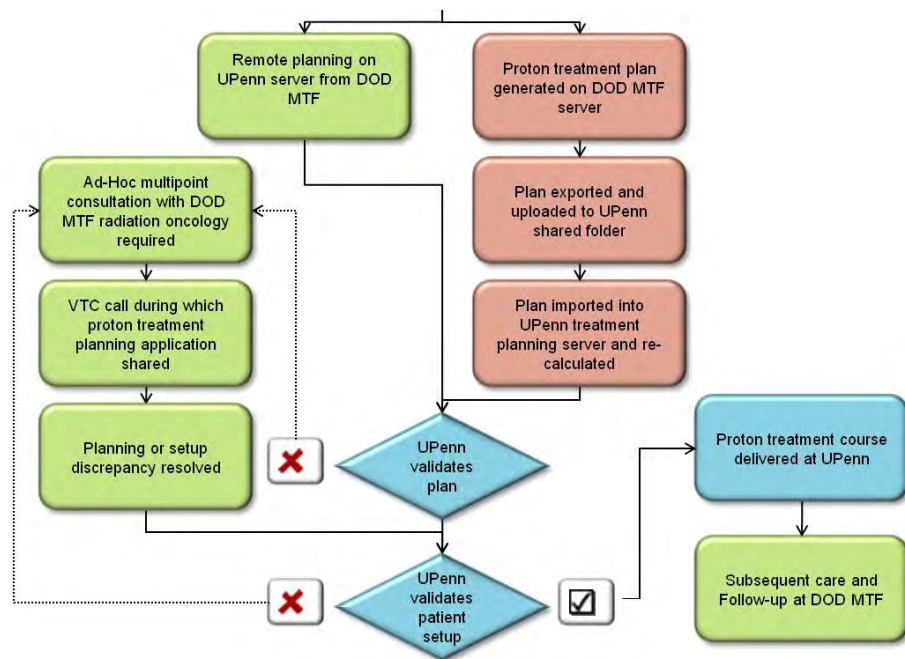
iii) A Feasibility Trial of Proton Radiation Therapy or Intensity Modulated Radiation Therapy Using Mild Hypofractionation for Intermediate-Risk Adenocarcinoma of the Prostate

Each trial takes the form of a Cooperative Research and Development Agreement (CRADA) between the University of Pennsylvania and the Walter Reed National Military Medical Center.

Because Department of Defense beneficiary data will be floating between the two institutions, a Data Sharing Agreement Application (DSAA) for each of these CRADAs had to be prepared and submitted to BUMED, to include a System Security Verification (SSV) questionnaire, which has taken a few months to put together. The three DSAs associated with the CRADAs listed above have been approved this quarter. Nine more are planned.

We hope that because our trials will essentially be using the same processes, our nine subsequent proton trials (CRADAs and accompanying DSAs/SSVs) will benefit from a speedier review process.

The SOP for remote treatment planning is shown in a diagram here:



The first DoD patient to be remotely planned using this system is scheduled for the first week of October.

#### 4). Administrative update

*Arnaud Belard*

a) The Program recruited Dr. Jessica Sheehan in MAR 2012, to fill the position of research scientist left vacant following the departure of Dr. Yu Chen. Dr. Sheehan was initially recruited as a research associate, pending the defense of her dissertation. During this transition, Ms. Sheehan was a part-time employee of the Program (24 hours a week). Following her defense in June, Dr. Sheehan transferred over to 'research scientist' status ; she transitioned to a full-time employee as well. Dr. Sheehan will be working specifically on organ/tumor motion management (one of the three pillars of our research). Her strong background in mechanical engineering is expected to be a great asset in designing a dynamic lung phantom, to be used for both phases five and six (please refer to Walter Reed research proposals for details).

b) A no-cost extension for USAMRAA contract W81XWH0720121 was approved. A recent analysis of our 'burn-rate' indicated that our funds for this phase would sustain our efforts until DEC 2012 ~ JAN 2013.

We recently became aware that a similar NCE was approved for contract W81XWH0920174 as we generated yet more 'surplus' during this period of performance. The accumulation of unspent funds is a result of savings attributed to delays in purchasing static and dynamic phantoms, and recruiting a new research scientist.

c) The Program added Jonathan Bear to its roster of co-investigators this quarter. A former Naval Aviator, Mr. Jonathan Bear is now a fourth year medical student at the Uniformed Services University of the Health Sciences (USUHS). He is expected to graduate this coming May (2012). Following a rotation at the Department of Radiation Oncology, Walter Reed National Military Medical Center (Bethesda, MD), Mr. Bear has expressed strong interest in a residency within our specialty (RadOnc, with a focus on proton therapy). Mr. Bear hopes to volunteer some of his time to assist in our research efforts. He will not be receiving any salary from the grant. He may be involved in research-related travel from time to time (conferences and off-site meetings pertaining to our program). We do not foresee any additional expenses for his participation in our research program.

d) Dr. Rulon Mayer's manuscript entitled 'Enhanced Dosimetry Procedures and Assessment for EBT2 Radiochromic Film' was accepted for publication (tentatively April 2012) in Medical Physics.

e) The Proton Beam Program Principal Investigator (COL John O'Connell) and a medical physicist (Ms. Yun-Hwa Wan) attended a two-week training course in early June for credentialing purposes (proton treatment planning for prostate and brain). This effort, while not funded via this cooperative-agreement (supported via funding from the United States Military Cancer Institute – Radiation Oncology Trials Program), directly supports the goal of ensuring Walter Reed providers (physicians and medical physicists) are qualified in proton radiotherapy planning (for which the telemedicine solution will be the vehicle).